

1 **OH-Initiated atmospheric degradation of hydroxyalkyl**  
2 **hydroperoxides: mechanism, kinetics, and structure-activity**  
3 **relationship**

4 Long Chen,<sup>1,2</sup> Yu Huang, <sup>\*</sup>1,2 Yonggang Xue, <sup>1,2</sup> Zhihui Jia, <sup>3</sup> Wenliang Wang<sup>4</sup>

5 <sup>1</sup> *State Key Lab of Loess and Quaternary Geology (SKLLQG), Institute of Earth*  
6 *Environment, Chinese Academy of Sciences (CAS), Xi'an, 710061, China*

7 <sup>2</sup> *CAS Center for Excellence in Quaternary Science and Global Change, Xi'an,*  
8 *710061, China*

9 <sup>3</sup> *School of Materials Science and Engineering, Shaanxi Normal University, Xi'an,*  
10 *Shaanxi, 710119, China*

11 <sup>4</sup> *School of Chemistry and Chemical Engineering, Key Laboratory for*  
12 *Macromolecular Science of Shaanxi Province, Shaanxi Normal University, Xi'an,*  
13 *Shaanxi, 710119, China*

14

15

16

17

18 Submitted to *Atmospheric Chemistry & Physics*

19

20

21 \*Corresponding author:

22 Prof. Yu Huang, E-mail address: [huangyu@ieecas.cn](mailto:huangyu@ieecas.cn)

23

24 **Abstract:**

25 Hydroxyalkyl hydroperoxides (HHPs), formed in the reactions of Criegee  
26 intermediates (CIs) with water vapour, play essential roles in the formation of  
27 secondary organic aerosol (SOA) under atmospheric conditions. However, the  
28 transformation mechanisms for OH-initiated oxidation of HHPs **remain** incompletely  
29 understood. Herein, the quantum chemical and kinetics modeling methods are applied  
30 to insight into the detailed mechanisms of OH-initiated oxidation of distinct HHPs  
31 (HOCH<sub>2</sub>OOH, HOCH(CH<sub>3</sub>)OOH and HOC(CH<sub>3</sub>)<sub>2</sub>OOH) formed from the reactions of  
32 CH<sub>2</sub>OO, *anti*-CH<sub>3</sub>CHOO and (CH<sub>3</sub>)<sub>2</sub>COO) with water vapor. The calculations show  
33 that the dominant pathway is the H-abstraction from the -OOH group in the initiation  
34 reactions of OH radical with HOCH<sub>2</sub>OOH and HOC(CH<sub>3</sub>)<sub>2</sub>OOH. H-abstraction from  
35 the -CH group is competitive with that from the -OOH group in the reaction of OH  
36 radical with HOCH(CH<sub>3</sub>)OOH. The barrier of H-abstraction from the -OOH group is  
37 slightly increased as the number of methyl group is increased. In pristine  
38 environments, the self-reaction of RO<sub>2</sub> radical initially produces tetroxide  
39 intermediate via an oxygen-to-oxygen coupling, then it decomposes into propagation  
40 and termination products through the asymmetric two-step O-O bond scission, in  
41 which the rate-limiting step is the first O-O bond cleavage. The barrier height of  
42 distinct **RO<sub>2</sub> radical reactions** with HO<sub>2</sub> radical is independent on the number of  
43 methyl substitution. In urban environments, reaction with O<sub>2</sub> forming formic acid and  
44 HO<sub>2</sub> radical is the dominant removal pathway for HOCH<sub>2</sub>O radical formed from the  
45 reaction of HOCH<sub>2</sub>OO radical with NO. The β-site C-C bond scission is the **dominant**  
46 pathway in the dissociation of HOCH(CH<sub>3</sub>)O and HOC(CH<sub>3</sub>)<sub>2</sub>O radicals formed from  
47 **the reactions of NO with HOCH(CH<sub>3</sub>)OO and HOC(CH<sub>3</sub>)<sub>2</sub>OO radicals**. These new  
48 findings are expected to deepen our current understanding for the photochemical  
49 oxidation of hydroperoxides under realistic atmospheric conditions.

50

## 51 **1. Introduction**

52 Hydroxyalkyl hydroperoxides (HHPs), formed in the reactions of Criegee  
53 intermediates (CIs) with water vapour and in the initiation OH-addition with  
54 subsequent HO<sub>2</sub>-termination reactions, play important roles in the formation of  
55 secondary organic aerosol (SOA) (Qiu et al., 2019; Kumar et al., 2014). The CIs  
56 formed from the ozonolysis of alkenes are characterized by high reactivity and excess  
57 energies, which can proceed either prompt unimolecular decay to OH radical or, after  
58 collisional stabilization, bimolecular reactions with various trace gases like SO<sub>2</sub>,  
59 NO<sub>2</sub> and H<sub>2</sub>O to produce sulfate, nitrate and SOA, thereby influencing air quality and  
60 human health (Lester and Klippenstein, 2018; Chen et al., 2017, 2019; Liu et al., 2019;  
61 Chhantyal-Pun et al., 2017; Anglada and Solé 2016; Gong and Chen, 2021). Among  
62 these reactions, the bimolecular reaction of CIs with water is thought to be the  
63 dominant chemical sink because its concentration ( $1.3\text{-}8.3 \times 10^{17}$  molecules cm<sup>-3</sup>) is  
64 several orders of magnitude greater than those of SO<sub>2</sub> and NO<sub>2</sub> ( $\sim 10^{12}$  molecules cm<sup>-3</sup>)  
65 in the atmosphere (Huang et al., 2015; Khan et al., 2018; Taatjes et al., 2013, 2017).  
66 The primary products of CIs reactivity toward water are highly oxygenated HHPs that  
67 are difficult to detect and identify by using the available analytical techniques due to  
68 their thermally instability (Qiu et al., 2019; Anglada and Solé 2016; Chao et al., 2015;  
69 Chen et al., 2016a; Ryzhkov and Ariya, 2003).

70 HHPs, due to the presence of both hydroxyl and perhydroxy moieties, have  
71 relatively low volatility contributing substantially to the formation of SOA (Qiu et al.,  
72 2019). The atmospheric degradation of HHPs initiated by OH radical is expected to be  
73 one of the dominant loss processes because OH radical is the most powerful oxidizing  
74 agent (Gligorovski et al., 2015; Allen et al., 2018). Reaction with OH radical includes  
75 three possible H-abstraction channels: (a) the alkyl hydrogen, (b) the -OH hydrogen,  
76 and (c) the -OOH hydrogen, which is followed by further reactions to generate  
77 organic peroxy radicals (RO<sub>2</sub>) as reactive intermediates (Allen et al., 2018). Based on  
78 our current mechanistic understanding, RO<sub>2</sub> radicals have three possible channels in  
79 pristine environments: (1) they can proceed self- and cross-reactions resulting in

80 formation of alkoxy radical RO, alcohol, carbonyl, accretion products (Berndt et al.,  
81 2018; Zhang et al., 2012; Valiev et al., 2019); (2) they can react with HO<sub>2</sub> radical  
82 leading to the formation of closed-shell hydroperoxide (ROOH), RO radical, OH  
83 radical, etc.; (Dillon and Crowley, 2008; Iyer et al., 2018) (3) they can undergo  
84 autoxidation via intramolecular H-shift and alternating O<sub>2</sub>-addition steps producing  
85 highly oxygenated organic molecules (HOMs), which have been identified as the low  
86 volatility compounds that contribute to the formation of SOA (Crouse et al., 2013;  
87 Jokinen et al., 2014; Wang et al., 2018; Ehn et al., 2014; Iyer et al., 2021). In urban  
88 environments, RO<sub>2</sub> radicals can react with NO<sub>x</sub> generating peroxyxynitrate (RO<sub>2</sub>NO<sub>2</sub>),  
89 organic nitrate (RONO<sub>2</sub>), RO radical and other SOA precursors (Wang et al., 2017;  
90 Xu et al., 2014, 2020; Ma et al., 2021). The relative importance of distinct pathways  
91 depends strongly on the nature of RO<sub>2</sub> radicals and the concentrations of coreactants.

92 Hydroxymethyl hydroperoxide (HMHP, HOCH<sub>2</sub>OOH), [the simplest HHPs come](#)  
93 [from the ozonolysis of all terminal alkenes in the presence of water](#), is observed in  
94 significant abundance in the atmosphere (Allen et al., 2018). The measured  
95 concentration of HMHP [is varied](#) considerably depending on the location, season and  
96 altitude, and its concentration is measured to be up to 5 ppbv in forested regions  
97 (Allen et al., 2018; Francisco and Eisfeld, 2009). Recently, the concentration of  
98 HMHP was measured during the summer 2013 in the southeastern United States, and  
99 found that the average mixing ratio of HMHP is 0.25 ppbv with a maximum of 4.0  
100 ppbv in the boundary layer (Allen et al., 2018). Allen et al. (2018) conducted the  
101 OH-initiated oxidation of HMHP in an environmental chamber and simulated the  
102 impact of HMHP oxidation on the global formic acid concentration using the  
103 chemical transport model GEOS-Chem. It was found that H-abstraction from the  
104 methyl group of HMHP results in formic acid, and it contributes to the global formic  
105 acid production about 1.7 Tg yr<sup>-1</sup>. Francisco and Eisfeld (2009) by employing *ab*  
106 *initio* CCSD(T)//MP2 methods, studied the atmospheric oxidation mechanism of  
107 HMHP initiated by OH radical, arriving at the same conclusion that the degradation of  
108 HMHP could be a new source of formic acid in the atmosphere. Additionally, the  
109 unimolecular decomposition of HMHP is another important removal process in the

110 atmosphere. Chen et al. (2016b) found that the formation of  $\text{CH}_2\text{O}$  and  $\text{H}_2\text{O}_2$  is more  
111 preferable than the production of  $\text{HCOOH}$  and  $\text{H}_2\text{O}$ . Kumar et al. (2014) obtained the  
112 same conclusion that the aldehyde- or ketone-forming pathway is kinetically favored  
113 over that the carboxylic acid-forming channel in the unimolecular decomposition of a  
114 variety of HHPs. All the above milestone investigations offer very useful information  
115 for understanding the decomposition of HHPs in the gas phase. However, to the best  
116 of our knowledge, [there are few studies](#) on the subsequent transformations of the  
117 resulting H-abstraction products formed from the OH-initiated oxidation of larger  
118 HHPs. The effect of the size and number of substituents on the rates and outcomes of  
119 SOA precursors (e.g. ROOR, HOMs) is uncertain up to now. Therefore, it is necessary  
120 to assess the potential of larger HHPs and their oxidation products to substantial SOA  
121 formation under different  $\text{NO}_x$  conditions.

122 In this article, we mainly investigate the detailed mechanisms and kinetic  
123 properties of distinct HHPs oxidation initiated by OH radical by employing quantum  
124 chemical and kinetics modeling methods. For the resulting H-abstraction products  
125  $\text{RO}_2$  radicals, the subsequent reactions involving self-reaction, isomerization and  
126 reaction with  $\text{HO}_2$  radical are taken into account in the absence of  $\text{NO}$ , while the  
127 subsequent reactions including addition, decomposition and H-abstraction by  $\text{O}_2$  are  
128 considered in the presence of  $\text{NO}$ . The investigated HHPs in this work are generated  
129 from the bimolecular reactions of distinct carbonyl oxides ( $\text{CH}_2\text{OO}$ , *anti*- $\text{CH}_3\text{CHOO}$   
130 and  $(\text{CH}_3)_2\text{COO}$ ) with water vapor.

## 131 **2. Computational details**

### 132 **2.1 Electronic structure and energy calculations**

133 The equilibrium geometries of all the open-shell species, including reactant (R),  
134 pre-reactive complex (RC), transition state (TS), post-reactive complex (PC), and  
135 product (P), are fully optimized at the unrestricted M06-2X/6-311+G(2df,2p) level of  
136 theory (UM06-2X) (Zhao and Truhlar, 2006; Zheng and Truhlar, 2009), whereas all  
137 the closed-shell species are optimized at the restricted M06-2X/6-311+G(2df,2p) level  
138 of theory (RM06-2X). This is because the M06-2X functional has been proven to

139 produce reliable performance for describing thermochemistry, kinetics and  
140 non-covalent interactions (Zhao and Truhlar, 2008). Harmonic vibrational frequencies  
141 are performed at the same level to verify that each stationary point is either a true  
142 minima (with no imaginary frequency) or a transition state (with one imaginary  
143 frequency). Zero-point vibrational energy (ZPVE) and Gibbs free energy corrections  
144 ( $G_{\text{corr}}$ ) from harmonic vibrational frequencies are scaled by a factor of 0.98 (Zhao and  
145 Truhlar, 2006). The intrinsic reaction coordinate (IRC) calculations are performed to  
146 verify the connection between the transition state and the designated reactant and  
147 product (Fukui, 1981). The single-point energies are calculated at the  
148 (U/R)M06-2X/ma-TZVP level of theory (Zheng, et al., 2011).

149 The tetroxide intermediate formed from the self-reaction of  $\text{RO}_2$  radical proceeds  
150 through the asymmetric two step O-O bond scission to produce a caged tetroxide  
151 intermediate of overall singlet multiplicity comprising two same-spin alkoxy radicals  
152 (spin down) and triplet oxygen (spin up). This type of reaction mechanism can be  
153 described by the broken symmetry unrestricted DFT (UDFT) and multi-reference  
154 CASSCF methods (Lee, et al., 2016; Bach, et al., 2005). Previous studies have  
155 demonstrated that the UDFT method is suitable to identify the minimum of metastable  
156 singlet caged radical complex and [the transition state of O-O bond homolysis](#), for  
157 which the energies are comparable to the more accurate and expensive CASSCF  
158 method (Lee, et al., 2016; Bach, et al., 2005). In the present study, the UDFT method  
159 is selected to study the asymmetric O-O bond scission and represents a compromise  
160 between the computational accuracy and efficiency. The broken symmetry  
161 UM06-2X/6-311+G(2df,2p) method is applied to generate the initial guesses of the  
162 tetroxide intermediate and transition state geometries with mixed HOMO and LUMO  
163 ( $S^2 \approx 1$ ) by using the guess = mix keyword. The single-point energies are refined at  
164 the UM06-2X/ma-TZVP level of theory.

165 In order to further evaluate the reliability of the employed method in predicting  
166 reaction mechanism, the single-point energies for all the stationary points involved in  
167 the initiation reactions of OH radical with distinct HHPs are recalculated at the  
168 (U/R)CCSD(T)/6-311+G(2df,2p) level of theory based on the (U/R)M06-2X

169 optimized geometries. Furthermore, the basis set superposition error (BSSE) is also  
170 performed to evaluate the stability of the pre-reactive complexes by employing the  
171 counterpoise method (Boys and Bernardi, 1970). For simplicity, no prefix is adopted  
172 throughout this article. Herein, the Gibbs free energy ( $G$ ) for each species is obtained  
173 by combining the single-point energy with the Gibbs correction ( $G = G_{\text{corr}} + E$ ). The  
174 electronic energy ( $\Delta E_a^\ddagger$ ) and free energy ( $\Delta G_a^\ddagger$ ) barriers are defined as the difference  
175 in energy between transition state and pre-reactive complex ( $\Delta E_a^\ddagger = E_{\text{TS}} - E_{\text{RC}}$  and  
176  $\Delta G_a^\ddagger = G_{\text{TS}} - G_{\text{RC}}$ ). The reaction free energy ( $\Delta G$ ) is referred to the difference in  
177 energy between product and reactant ( $\Delta G = G_{\text{P}} - G_{\text{R}}$ ). The calculated  $\Delta E_a^\ddagger$  and  $\Delta G_a^\ddagger$   
178 for the initiation H-abstraction pathways are summarized in Table S1. As shown in  
179 Table S1, the mean absolute deviations (MADs) of  $\Delta E_a^\ddagger$  and  $\Delta G_a^\ddagger$  between  
180 CCSD(T)/6-311+G(2df,2p) and M06-2X/ma-TZVP approaches are 0.43 and 0.45  
181 kcal mol<sup>-1</sup>, respectively; the largest deviations of  $\Delta E_a^\ddagger$  and  $\Delta G_a^\ddagger$  are 1.2 and 1.1  
182 kcal mol<sup>-1</sup>, respectively. These results reveal that the energies obtained from the  
183 M06-2X/ma-TZVP method are in very good accord with those from the gold-standard  
184 coupled-cluster approach CCSD(T) within the uncertainties of systematic errors.  
185 Therefore, the M06-2X/ma-TZVP method is selected to investigate the atmospheric  
186 degradation of HHP initiated by OH radical under different conditions. In the  
187 following sections, unless otherwise stated, the  $\Delta G_a^\ddagger$  is applied to construct the  
188 reaction profiles.

189 For the H-shift reactions of RO<sub>2</sub> radicals, reactants, transition states and products  
190 have multiple conformers. [Previous literature has demonstrated](#) that the reaction  
191 kinetics of multiconformers involvement are more precisely than that of the single  
192 conformer approximation (Møller, et al., 2016, 2020). Herein, the [multiconformer](#)  
193 treatment is performed to investigate the H-shift reactions of RO<sub>2</sub> radicals. A  
194 conformer search within the Molclus program is employed to generate a pool of  
195 conformers for RO<sub>2</sub> radicals (Lu, 2020). The selected conformers are further  
196 optimized at the M06-2X/6-311+G(2df,2p) level of theory, followed by single-point  
197 energy calculations at the M06-2X/ma-TZVP level of theory. On the basis of the  
198 calculated Gibbs free energies, the Boltzmann populations ( $w_i$ ) of each RO<sub>2</sub>

199 conformer is expressed as eqn 1.

$$200 \quad w_i = \frac{e^{-\Delta G_i/k_B T}}{\sum_i e^{-\Delta G_i/k_B T}} \quad (1)$$

201 where  $\Delta G_i$  is the relative Gibbs free energy of conformer  $i$ ,  $k_B$  is the Boltzmann's  
202 constant,  $T$  is temperature in Kelvin. All the quantum chemical calculations are  
203 performed by using the Gaussian 09 program package (Frisch, et al., 2009).

## 204 **2.2 Kinetics calculations**

205 The rate coefficients of unimolecular reactions are calculated by using the  
206 Rice-Ramsperger-Kassel-Marcus theory coupled with energy-grained master equation  
207 (RRKM-ME) method (Holbrook, 1996), and the rate coefficients of bimolecular  
208 reactions are determined by utilizing traditional transition state theory (TST)  
209 (Fernández-Ramos, 2007). The RRKM-ME calculations are performed by  
210 implementing the MESMER 6.0 program suite (Glowacki, et al., 2012).  $N_2$  is used as  
211 the buffer gas. The single exponential down model is employed to simulate the  
212 collision energy transfer ( $\langle \Delta E \rangle_{\text{down}} = 200 \text{ cm}^{-1}$ ). The collisional Lennard-Jones  
213 parameters are estimated by using an empirical formula described by Gilbert and  
214 Smith (1990). For the H-shift reactions of  $RO_2$  radicals, the rate coefficients are  
215 determined by employing the multiconformer transition state theory (MC-TST)  
216 approach (Møller, et al., 2016). The MC-TST rate coefficient  $k_{\text{MC-TST}}$  is calculated by  
217 the sum of the individual intrinsic reaction coordinate TST (IRC-TST) rate coefficient  
218  $k_{\text{IRC-TST}}$ , each weighted by Boltzmann population of corresponding  $RO_2$  conformer  
219 (Møller, et al., 2016).

$$220 \quad k_{\text{MC-TST}} = \sum_i^{\text{all TS conf.}} w_i \times k_{\text{IRC-TST}i} \quad (2)$$

221 where  $k_{\text{IRC-TST}i}$  represents the rate coefficient of conformer  $i$ , and  $w_i$  is the relative  
222 Boltzmann population of the corresponding reactant connected to  $TS_i$ . The  
223 one-dimensional asymmetry Eckart model is employed to calculate the tunneling  
224 correction (Eckart, 1930). Considering the uncertainty in barrier heights ( $\sim 1.0$   
225  $\text{kcal mol}^{-1}$  by the M06-2X method) and in tunneling corrections, the uncertainty of the



249 and  $-O_2O_3H_2$  groups (R4). For each pathway, a pre-reactive complex with a six- or  
250 seven-membered ring structure is formed in the entrance channel, which is stabilized  
251 by hydrogen bond interactions between the oxygen atom of OH radical and the  
252 abstraction hydrogen atom of HOCH<sub>2</sub>OOH, and the remnant hydrogen atom of OH  
253 radical and one of oxygen atoms of HOCH<sub>2</sub>OOH (Figure S6). Then, it surmounts  
254 modest barrier that is higher in energy than the reactants to reaction. The reaction  
255 barriers  $\Delta G_a^\ddagger$  are reduced in the order of 6.4 (R1) > 5.8 (R2)  $\approx$  5.4 (R3) > 1.5 (R4)  
256 kcal mol<sup>-1</sup>, indicating that H-abstraction from the  $-O_2O_3H_2$  group (R4) is more  
257 preferable than those from the  $-O_1H_1$ ,  $-C_1H_3$  and  $-C_1H_4$  groups (R1-R3). The same  
258 conclusion is also derived from the energy barriers  $\Delta E_a^\ddagger$  that R4 is the most favorable  
259 H-abstraction pathway (Figure S1). The difference of barrier heights can be attributed  
260 to the bond dissociation energy (BDE) of different types of bonds in HOCH<sub>2</sub>OOH  
261 molecule. The BDE decrease in the order of 103.7 ( $O_1-H_1$ ) > 98.2 ( $C_1-H_3$ )  $\approx$  97.4  
262 ( $C_1-H_4$ ) > 87.2 ( $O_3-H_2$ ) kcal mol<sup>-1</sup>, which are in good agreement with the order of  
263 barrier heights of H-abstraction reactions. As indicated by their reaction free energy  
264 values, it can be found that the exothermicity of R4 is the largest among these four  
265 H-abstraction reactions. Based on the above discussions, it is concluded that  
266 H-abstraction from the  $-O_2O_3H_2$  group resulting in formation of HOCH<sub>2</sub>OO radical  
267 (R4) is feasible on both thermodynamically and kinetically.

268 Considering the different reaction sites of hydrogen atoms, the atmospheric  
269 transformation of HOCH(CH<sub>3</sub>)OOH from the *anti*-CH<sub>3</sub>CHOO + H<sub>2</sub>O reaction should  
270 have six possible H-abstraction pathways as presented in Figure 3. As shown in  
271 Figure 3, each H-abstraction reaction begins with the formation of a weakly bound  
272 hydrogen bonded pre-reactive complex with a six- or seven-membered ring structure  
273 in the entrance channel (Figure S7). Then it immediately transforms into the  
274 respective product via the corresponding transition state. The  $\Delta G_a^\ddagger$  of H-abstraction  
275 from the  $-C_1H_3$  (R6) and  $-O_2O_3H_2$  (R8) groups are 2.2 and 1.7 kcal mol<sup>-1</sup>, respectively,  
276 which are  $\sim$  4-5 kcal mol<sup>-1</sup> lower than those from the  $-O_1H_1$  (R5) and  $-CH_3$  groups  
277 (R7). This result shows that R6 and R8 have nearly identical importance in the  
278 atmosphere. Compared with the barriers of H-abstraction at the  $C_\alpha$  (R6) and  $C_\beta$  (R7)

279 positions, it can be found that the former case is more favourable than the latter case.  
280 This conclusion is further supported by Jara-Toro's study for the reactions of OH  
281 radical with linear saturated alcohols (methanol, ethanol and n-propanol) that  
282 H-abstraction at the C<sub>α</sub> position is predominant (Jara-Toro, et al., 2017, 2018).

283 For the OH-initiated oxidation of HOCH(CH<sub>3</sub>)OOH from the *syn*-CH<sub>3</sub>CHOO +  
284 H<sub>2</sub>O reaction, the corresponding free-energy and electronic-energy PESs are  
285 displayed in Figures S4 and S5, respectively. From Figure S4, it can be seen the  
286 H-abstraction by OH radical from HOCH(CH<sub>3</sub>)OOH has six possible pathways. For  
287 each pathway, a pre-reactive complex is formed prior to the corresponding transition  
288 state, and then it overcomes modest barrier to reaction. The  $\Delta G_a^\ddagger$  of R6' and R8' are  
289 2.3 and 1.8 kcal mol<sup>-1</sup>, respectively, which are about 5 kcal mol<sup>-1</sup> lower than those of  
290 R5' and R7'. This result shows that H-abstraction from the -CH (R6') and -OOH (R8')  
291 groups are preferable kinetically. **The same conclusion** is also derived from the energy  
292 barriers  $\Delta E_a^\ddagger$  that the R6' and R8' are the most favourable H-abstraction pathways  
293 (Figure S5). It should be noted that although the barriers of R6' and R8' are  
294 comparable, the exoergicity of the former case is significantly lower than that of the  
295 latter case. The above-mentioned conclusions are consistent with the results derived  
296 from the OH-initiated oxidation of HOCH(CH<sub>3</sub>)OOH from the *anti*-CH<sub>3</sub>CHOO +  
297 H<sub>2</sub>O reaction. Zhou et al. has demonstrated that the bimolecular reaction of  
298 *syn*-CH<sub>3</sub>CHOO with water leading to the formation of HOCH(CH<sub>3</sub>)OOH is of less  
299 importance in the atmosphere, while the unimolecular decay to OH radical is the  
300 major loss process of *syn*-CH<sub>3</sub>CHOO (Zhou et al., 2019). Therefore, in the present  
301 study, we mainly focus on the subsequent mechanism of intermediate generated from  
302 OH-initiated oxidation of HOCH(CH<sub>3</sub>)OOH from the *anti*-CH<sub>3</sub>CHOO + H<sub>2</sub>O  
303 reaction.

304 From Figure 4, it can be seen that H-abstraction from HOC(CH<sub>3</sub>)<sub>2</sub>OOH  
305 includes eight possible H-abstraction pathways. All the H-abstraction reactions are  
306 strongly exothermic and spontaneous, signifying that they are thermodynamically  
307 feasible under atmospheric conditions. It deserves mentioning that the release of  
308 energy of R12 is significantly greater than those of R9-R11. For each H-abstraction

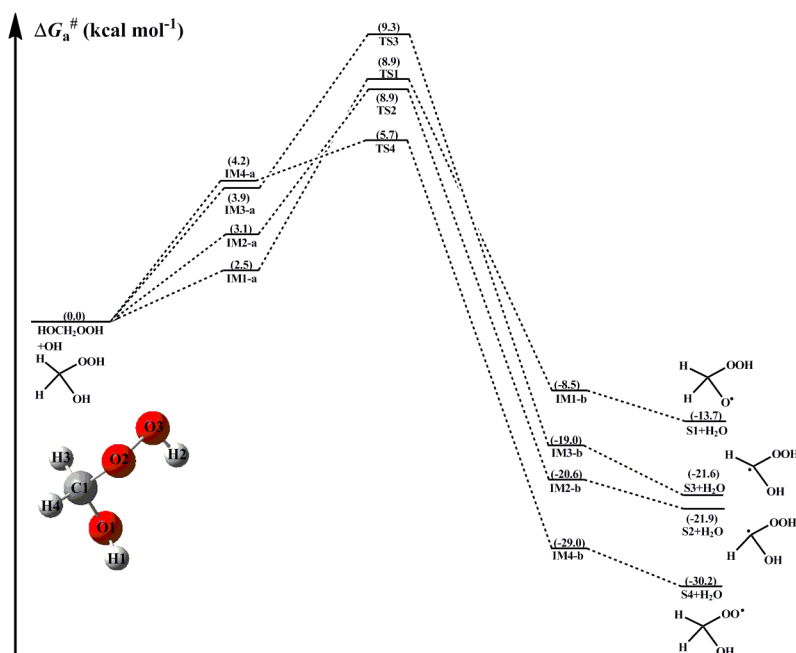
309 pathway, a RC with a six- or seven-membered ring structure is formed prior to the  
310 corresponding TS, which is more stable than the separate reactants due to the  
311 hydrogen bond interactions between  $\text{HOC}(\text{CH}_3)_2\text{OOH}$  and OH radical. Then, the RC  
312 overcomes modest barrier to reaction. The  $\Delta G_a^\ddagger$  of H-abstraction from the  $-\text{O}_2\text{O}_3\text{H}_2$   
313 group (R12) is  $2.7 \text{ kcal mol}^{-1}$ , which is the lowest among these eight H-abstraction  
314 reactions. This result again shows that the H-abstraction from the  $-\text{O}_2\text{O}_3\text{H}_2$  group is  
315 the dominant pathway.

316 The rate coefficients of every H-abstraction pathway involved in the initiation  
317 reactions of distinct HHPs with OH radical are estimated over the temperature range  
318 from 273 to 400 K as summarized in Table S2-S4 and Figures S9-S11. As shown in  
319 Table S2, the total rate coefficients  $k_{\text{tot}}$  of  $\text{HOCH}_2\text{OOH}$  reaction with OH radical  
320 decrease slightly with increasing temperature. At ambient temperature,  $k_{\text{tot}}$  is  
321 estimated to be  $3.3 \times 10^{-11} \text{ cm}^3 \text{ molecule}^{-1} \text{ s}^{-1}$ , which is a factor of  $\sim 5$  greater than the  
322 Allen's result ( $(7.1 \pm 1.5) \times 10^{-12} \text{ cm}^3 \text{ molecule}^{-1} \text{ s}^{-1}$ , at 295 K) derived from the  
323 reaction of HMHP with OH radical by using the  $\text{CF}_3\text{O}^-$  chemical ionization mass  
324 spectrometry (CIMS) and laser-induced fluorescence (LIF) (Allen, et al., 2018). Such  
325 a discrepancy could be attributed to the uncertainty in barrier height and tunneling  
326 correction.  $k_{\text{R4}(\text{O3-H2})}$  is 1-2 orders of magnitude greater than  $k_{\text{R1}(\text{O1-H1})}$ ,  $k_{\text{R2}(\text{C1-H3})}$  and  
327  $k_{\text{R3}(\text{C1-H4})}$  in the whole temperature range, implying that R4 is the most favorable  
328 H-abstraction pathway. For example,  $k_{\text{R4}(\text{O3-H2})}$  is calculated to be  $2.9 \times 10^{-11} \text{ cm}^3$   
329  $\text{molecule}^{-1} \text{ s}^{-1}$  at 298 K, which is higher than  $k_{\text{R1}(\text{O1-H1})}$  ( $1.8 \times 10^{-13}$ ),  $k_{\text{R2}(\text{C1-H3})}$  ( $9.9 \times$   
330  $10^{-13}$ ) and  $k_{\text{R3}(\text{C1-H4})}$  ( $2.0 \times 10^{-12}$ ) by 161, 29 and 15 times, respectively.

331 From Table S3, it can be seen that the total rate coefficients  $k'_{\text{tot}}$  of  
332  $\text{HOCH}(\text{CH}_3)\text{OOH}$  reaction with OH radical decrease in the range of  $4.5 \times 10^{-11}$  (273  
333 K) to  $8.1 \times 10^{-12}$  (400 K)  $\text{cm}^3 \text{ molecule}^{-1} \text{ s}^{-1}$  with increasing temperature, and they  
334 exhibit a slightly negative temperature dependence.  $k_{\text{R8}(\text{O3-H2})}$  are approximately  
335 identical to  $k'_{\text{tot}}$  in the entire temperature range, which are 1-2 orders of magnitude  
336 greater than  $k_{\text{R5}(\text{O1-H1})}$ ,  $k_{\text{R6}(\text{C1-H3})}$ ,  $k_{\text{R7-1}(\text{C2-H4})}$ ,  $k_{\text{R7-2}(\text{C2-H5})}$  and  $k_{\text{R7-3}(\text{C2-H6})}$ . The result again  
337 shows that H-abstraction from the  $-\text{OOH}$  group (R8) is preferable kinetically. It  
338 should be noted that although the barriers of R8 and R6 are comparable,  $k_{\text{R8}(\text{O3-H2})}$  is

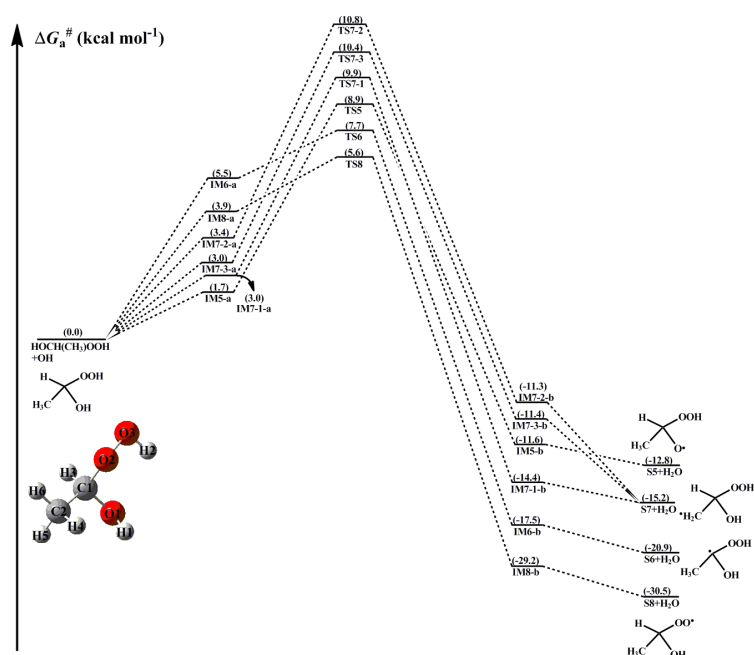
339 about one order of magnitude higher than  $k_{R6(C1-H3)}$  over the temperature range studied.  
340 The most likely reason is due to the stability of pre-reactive complexes that IM8-a is  
341 more stable than IM6-a in energy. A similar conclusion is derived from the results of  
342 rate coefficients of  $\text{HOC}(\text{CH}_3)_2\text{OOH} + \text{OH}$  reaction that H-abstraction from the -OOH  
343 group (R12) is favorable kinetically (Table S4). The atmospheric lifetime of  
344  $\text{HOCH}_2\text{OOH}$ ,  $\text{HOCH}(\text{CH}_3)\text{OOH}$  and  $\text{HOC}(\text{CH}_3)_2\text{OOH}$  reactivity toward OH radical  
345 are estimated to be 0.58-1.74 h, 0.60-1.79 h and 1.23-3.69 h at room temperature  
346 under typical OH radical concentrations of  $5\text{-}15 \times 10^6$  molecules  $\text{cm}^{-3}$  during daylight  
347 (Long et al., 2017).

348 In summary, the dominant pathway is the H-abstraction from the -OOH group in  
349 the initiation reactions of OH radical with  $\text{HOCH}_2\text{OOH}$ . H-abstraction from the -CH  
350 group is competitive with that from the -OOH group in the reaction of OH radical  
351 with  $\text{HOCH}(\text{CH}_3)\text{OOH}$ . Compared with the barriers of H-abstraction from the -OOH  
352 and -CH<sub>2</sub> groups in the reaction of OH radical with  $\text{HOCH}_2\text{OOH}$ , it can be found  
353 that the barrier of H-abstraction from the -CH group is reduced by  $3.6 \text{ kcal mol}^{-1}$ ,  
354 whereas the barrier of H-abstraction from the -OOH group is increased by  $0.2$   
355  $\text{kcal mol}^{-1}$  when a methyl group substitution occurs at the C1-position of  
356  $\text{HOCH}_2\text{OOH}$ . The dominant pathway is the H-abstraction from the -OOH group in  
357 the reaction of OH radical with  $\text{HOC}(\text{CH}_3)_2\text{OOH}$ , and the barrier height is increased  
358 by  $1.2 \text{ kcal mol}^{-1}$  compared to the OH +  $\text{HOCH}_2\text{OOH}$  system. The barrier of  
359 H-abstraction from the -OOH group is slightly increased as the number of methyl  
360 group is increased. It is interesting to compare the rate coefficient of dominant  
361 pathway in the OH +  $\text{HOCH}_2\text{OOH}$  system with that for the analogous reactions in  
362 the OH +  $\text{HOCH}(\text{CH}_3)\text{OOH}$  and OH +  $\text{HOC}(\text{CH}_3)_2\text{OOH}$  reactions. It can be found  
363 that the rate coefficient is almost identical when a methyl group substitution occurs  
364 at the C<sub>1</sub>-position, whereas the rate coefficient reduces by a factor of 2-5 when two  
365 methyl groups are introduced into the C<sub>1</sub>-position.



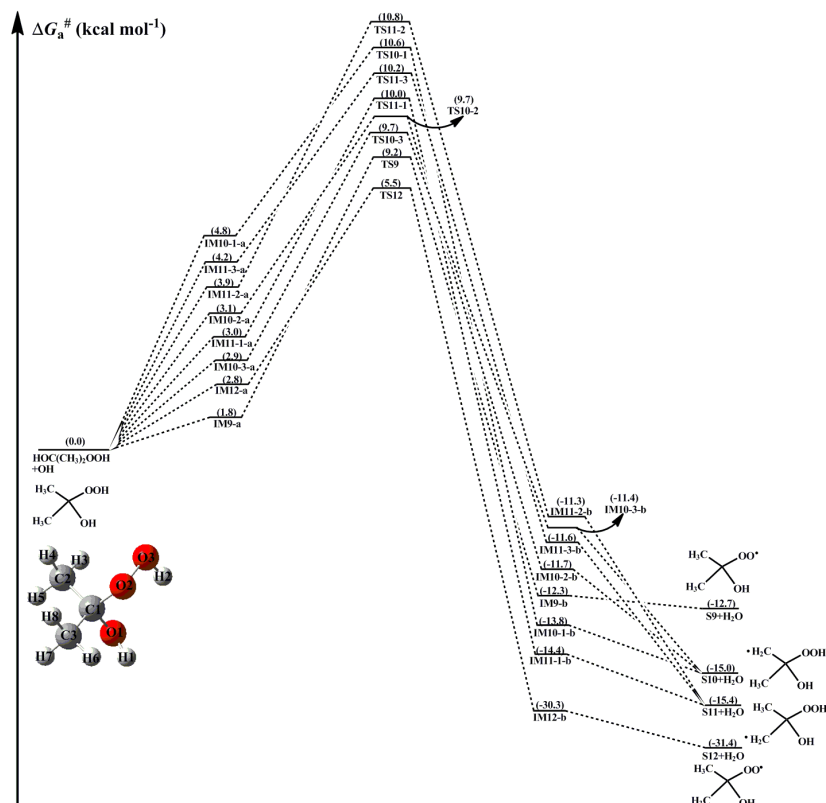
366

367 **Figure 2.** PES ( $\Delta G_a^\ddagger$ ) for the OH-initiated reactions of HOCH<sub>2</sub>OOH from the CH<sub>2</sub>OO + H<sub>2</sub>O  
 368 reaction predicted at the M06-2X/ma-TZVP//M06-2X/6-311+G(2df,2p) level of theory (a and b  
 369 represent the pre-reactive and post-reactive complexes)



370

371 **Figure 3.** PES ( $\Delta G_a^\ddagger$ ) for the OH-initiated reactions of HOCH(CH<sub>3</sub>)OOH from the  
 372 *anti*-CH<sub>3</sub>CHOO + H<sub>2</sub>O reaction predicted at the M06-2X/ma-TZVP//M06-2X/6-311+G(2df,2p)  
 373 level of theory (a and b represent the pre-reactive and post-reactive complexes)



374

375 **Figure 4.** PES ( $\Delta G_a^\ddagger$ ) for the OH-initiated reactions of HOC(CH<sub>3</sub>)<sub>2</sub>OOH from the (CH<sub>3</sub>)<sub>2</sub>COO +  
 376 H<sub>2</sub>O reaction predicted at the M06-2X/ma-TZVP//M06-2X/6-311+G(2df,2p) level of theory (a  
 377 and b represent the pre-reactive and post-reactive complexes)

### 378 3.2 Subsequent reactions of H-abstraction products RO<sub>2</sub> radicals 379 in pristine environments

380 In principle, the H-abstraction products RO<sub>2</sub> radicals [have three possible fates in](#)  
 381 [pristine environments](#): (1) the self-reactions of RO<sub>2</sub> radicals can either produce RO +  
 382 R'O + O<sub>2</sub> (propagation channel), or generate ROH + R'(-H, =O) + O<sub>2</sub> or produce  
 383 ROOR + O<sub>2</sub> (termination channel) that has been recognized as an important SOA  
 384 precursor (Berndt et al., 2018; Zhang et al., 2012); (2) RO<sub>2</sub> radicals react with HO<sub>2</sub>  
 385 radical leading to the formation of hydroperoxide ROOH, alcohol, OH and other  
 386 products (Winiberg et al., 2016; Chen et al., 2021); (3) RO<sub>2</sub> radicals autoxidation  
 387 through intramolecular H-shift and alternating O<sub>2</sub> addition steps generate HOMs (Ehn  
 388 et al., 2014; Bianchi et al., 2019; Nozière and Vereecken, 2019; Rissanen et al., 2014).  
 389 The relevant details for these three kinds of reactions will be discussed in the  
 390 following paragraph.

### 3.2.1 Reactions mechanism for the self-reaction of RO<sub>2</sub> radicals

The self-reaction is one of dominant removal pathways for RO<sub>2</sub> radicals when the concentration of NO is low and the concentration of RO<sub>2</sub> radicals is high. The self-reaction of RO<sub>2</sub> radicals usually follows the Russell mechanism (Russell, 1957), and mainly includes four possible pathways: (1)  $2\text{RO}_2 \rightarrow 2\text{RO} + \text{O}_2$ ; (2)  $2\text{RO}_2 \rightarrow \text{ROH} + \text{R}'\text{CO} + \text{O}_2$ ; (3)  $2\text{RO}_2 \rightarrow \text{ROOR} + \text{O}_2$ ; (4)  $2\text{RO}_2 \rightarrow \text{ROOH} + \text{R}'\text{CHOO}$  (Atkinson and Arey, 2003). The relative importance of different pathways is varied considerably depending on the nature of RO<sub>2</sub> radicals (Valiev et al., 2019; Lee et al., 2016). A schematic PES for the self-reaction of HOCH<sub>2</sub>OO radical is drawn in Figure 5. As can be seen in Figure 5a, the self-reaction of HOCH<sub>2</sub>OO radical starts with the formations of tetroxide complexes IM13-a and IM14-a in the entrance channel, with 2.9 and 3.4 kcal mol<sup>-1</sup> stability. Then they fragment into dimer S13 + <sup>1</sup>O<sub>2</sub> (R13) and HOCH<sub>2</sub>OOH + HOCHOO (R14) via transition states TS13 and TS14 with the barriers of 43.3 and 51.5 kcal mol<sup>-1</sup>. But the barriers of R13 and R14 are extremely high, making them irrelevant in the atmosphere.

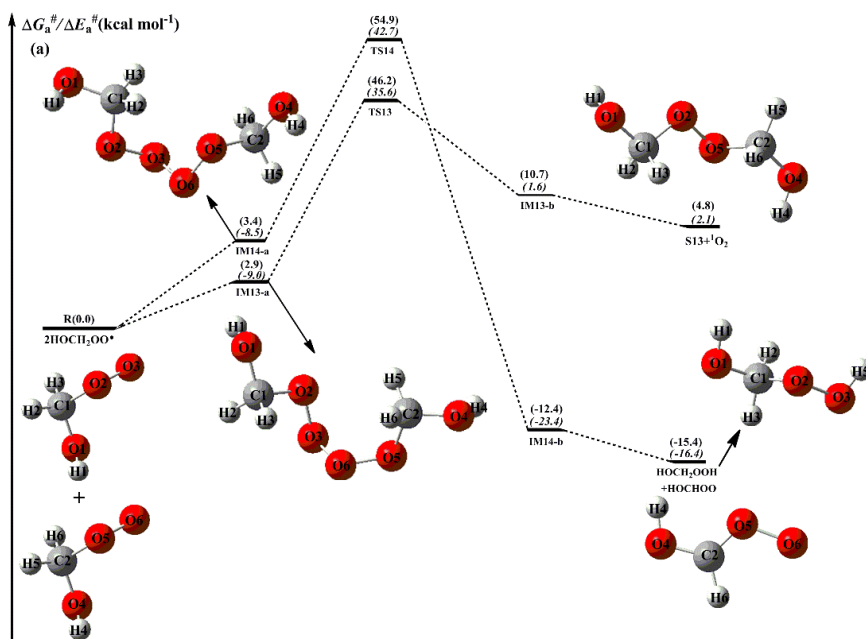
From Figure 5b, it is seen that the self-reaction of HOCH<sub>2</sub>OO radical proceeds via oxygen-to-oxygen coupling leading to the formation of tetroxide intermediate S14 with the electronic energy and free energy barriers of 7.3 and 19.6 kcal mol<sup>-1</sup>. Kumar and Francisco reported that the electronic energy barrier of the gas phase decomposition of HOCH<sub>2</sub>OO radical is 14.0 kcal mol<sup>-1</sup> and it could be a new source of HO<sub>2</sub> radical in the troposphere (Kumar and Francisco, 2015, 2016). Compared with the electronic energy barriers of unimolecular dissociation of HOCH<sub>2</sub>OO radical and its self-reaction, it can be found that the self-reaction of HOCH<sub>2</sub>OO radical resulting in formation of S14 is significantly feasible. The formed S14 can fragment into HOCH<sub>2</sub>O + HCOOH + HO<sub>2</sub> via a concerted process of O<sub>2</sub>-O<sub>3</sub> and O<sub>5</sub>-O<sub>6</sub> bonds rupture and O<sub>3</sub>-H<sub>6</sub> bond forming with the barrier of 29.8 kcal mol<sup>-1</sup>. Alternatively, S14 can convert into the caged tetroxide intermediate S16 through the asymmetric two step O<sub>2</sub>-O<sub>3</sub> and O<sub>5</sub>-O<sub>6</sub> bonds scission with the barriers of 19.1 and 3.1 kcal mol<sup>-1</sup>, respectively. The result shows that the latter pathway is more preferable than the

420 former channel owing to its lower barrier. The overall spin multiplicity of S16 is  
421 singlet, in which the O<sub>2</sub> moiety maintains the triplet ground state (spin up) and is very  
422 loosely bound. In order to preserve the overall singlet multiplicity, the two HOCH<sub>2</sub>O  
423 radical pairs (<sup>3</sup>(HOCH<sub>2</sub>O ··HOCH<sub>2</sub>O)) must have the triplet multiplicity (spin down).  
424 S16 could be regarded as the ground state <sup>3</sup>O<sub>2</sub> moving away from the two HOCH<sub>2</sub>O  
425 radical pairs that keep interacting. Due to the difficulty in performing the constrained  
426 optimization for the dissociation of S16, the <sup>3</sup>O<sub>2</sub> moiety is considered as a leaving  
427 moiety away from two HOCH<sub>2</sub>O radical pairs, and merely the dissociation of  
428 <sup>3</sup>(HOCH<sub>2</sub>O ··HOCH<sub>2</sub>O) is taken into consideration in the present study. It has three  
429 types of pathways: (1) it yields HOCH<sub>2</sub>OH and excited-state <sup>3</sup>HCOOH through the  
430 alpha hydrogen transfer with the barrier of 14.0 kcal mol<sup>-1</sup> and 10.2 kcal mol<sup>-1</sup>  
431 exothermicity, followed by the excited <sup>3</sup>HCOOH to go back to the ground-state  
432 <sup>1</sup>HCOOH; (2) it generates two HOCH<sub>2</sub>O radicals via the barrierless process with the  
433 exoergicity of 16.9 kcal mol<sup>-1</sup>; (3) it produces dimer S17 via an intersystem crossing  
434 (ISC) step with the exoergicity of 32.1 kcal mol<sup>-1</sup>. Based on the calculated reaction  
435 barriers, it can be found that the rate-limiting step is the cleavage of O<sub>2</sub>-O<sub>3</sub> bond (R17)  
436 in the unimolecular decay processes of S14. This conclusion coincides with the  
437 previous result obtained from the dissociation of di-t-butyl tetroxide that the  
438 rate-controlling step is the rupture of single O-O bond (Lee et al., 2016). Valiev et al.  
439 (2019) proposed that the ISC rate of ROOR dimer formed from the different  
440 (RO ··R'O) systems is extremely rapid (> 10<sup>8</sup> s<sup>-1</sup>) and exhibits a strong  
441 stereoselectivity.

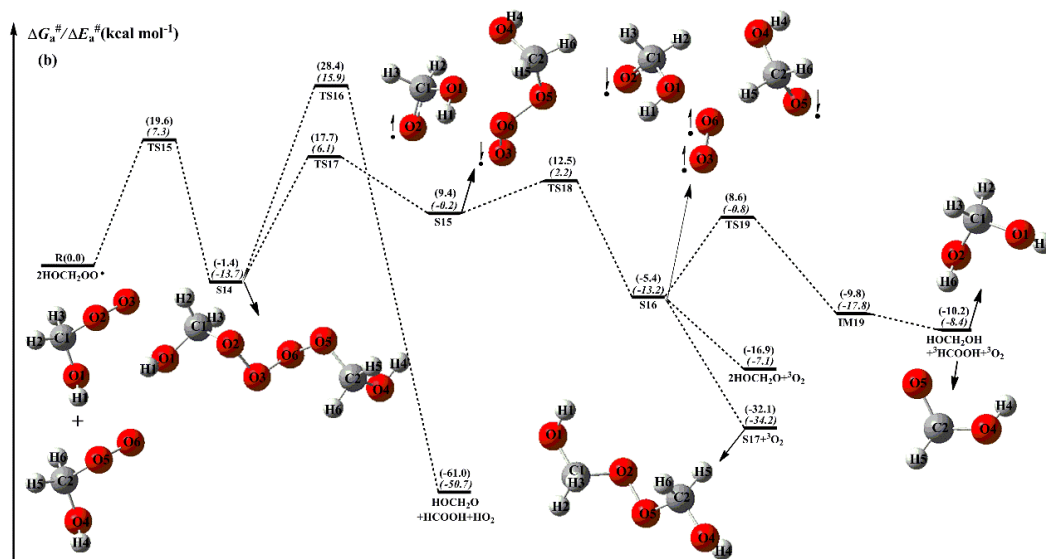
442 Figure 6 depicts a schematic PES for the self-reaction of HOCH(CH<sub>3</sub>)OO radical.  
443 As shown in Figure 6a, the self-reaction of HOCH(CH<sub>3</sub>)OO radical can either  
444 produce dimer S18 along with <sup>1</sup>O<sub>2</sub> via transition state TS20 with the barrier of 44.4  
445 kcal mol<sup>-1</sup>, or generate HOCH(CH<sub>3</sub>)OOH and HOC(CH<sub>3</sub>)OO through transition state  
446 TS21 with the barrier of 54.3 kcal mol<sup>-1</sup>. But the barriers of R20 and R21 are  
447 significantly high, making them of less importance in the atmosphere. Alternatively,  
448 the self-reaction of HOCH(CH<sub>3</sub>)OO radical proceeds via an oxygen-to-oxygen  
449 coupling resulting in formation of tetroxide intermediate S19 with the barrier of 19.9

450 kcal mol<sup>-1</sup> (Figure 6b). The formed S19 proceeds through the asymmetric two step  
451 O<sub>2</sub>-O<sub>3</sub> and O<sub>5</sub>-O<sub>6</sub> bonds scission to produce a caged tetroxide intermediate S21 of  
452 overall singlet multiplicity comprising two same-spin alkoxy radicals (spin down)  
453 and triplet oxygen (spin up). These two processes overcome the barriers of 21.4 and  
454 1.3 kcal mol<sup>-1</sup>, respectively. Then, S21 decomposes into the propagation  
455 (2HOCH(CH<sub>3</sub>)O + <sup>3</sup>O<sub>2</sub>) and termination products (HOCH(CH<sub>3</sub>)OH + <sup>3</sup>CH<sub>3</sub>OOH +  
456 <sup>3</sup>O<sub>2</sub> and dimer S22 + <sup>3</sup>O<sub>2</sub>) with the exoergicity of 12.5, 11.7 and 33.0 kcal mol<sup>-1</sup>. The  
457 rate-determining step is the rupture of O<sub>2</sub>-O<sub>3</sub> bond (R24) in the dissociation processes  
458 of S19.

459 As shown in Figure 7, the dominant pathway for the self-reaction of  
460 HO(CH<sub>3</sub>)<sub>2</sub>COO radical begins with the formation of tetroxide intermediate S24 via an  
461 oxygen-to-oxygen coupling transition state TS28 with the barrier of 20.4 kcal mol<sup>-1</sup>;  
462 then it transforms into the caged tetroxide intermediate S26 of overall singlet spin  
463 multiplicity through the asymmetric two-step O-O bond cleavage with the barriers of  
464 22.0 and 3.4 kcal mol<sup>-1</sup>; finally, S26 can either produce two HO(CH<sub>3</sub>)<sub>2</sub>CO radicals  
465 with the exoergicity of 10.3 kcal mol<sup>-1</sup>, or generate dimer S27 with the exothermicity  
466 of 31.5 kcal mol<sup>-1</sup>. Compared with the self-reactions of HOCH<sub>2</sub>OO and  
467 HOCH(CH<sub>3</sub>)OO radicals, it can be found that the termination product of the  
468 self-reaction of HOC(CH<sub>3</sub>)<sub>2</sub>OO radical is exclusively dimer S27. The reason is due to  
469 the absence of alpha hydrogen atom in HOC(CH<sub>3</sub>)<sub>2</sub>OO radical. Compared with the  
470 barrier of rate-determining route R17 in the self-reaction of HOCH<sub>2</sub>OO radical, it can  
471 be found that the barrier of rate-limiting step R29 is increased by about 3.0 kcal mol<sup>-1</sup>  
472 when two methyl substitutions are introduced into the C1-position of HOCH<sub>2</sub>OO  
473 radical. The reason might be attributed to the cage escape of alkoxy radicals. It is  
474 therefore that the tertiary RO<sub>2</sub> radicals have great opportunity to react with HO<sub>2</sub>  
475 radical or undergo autoxidation in pristine environments.



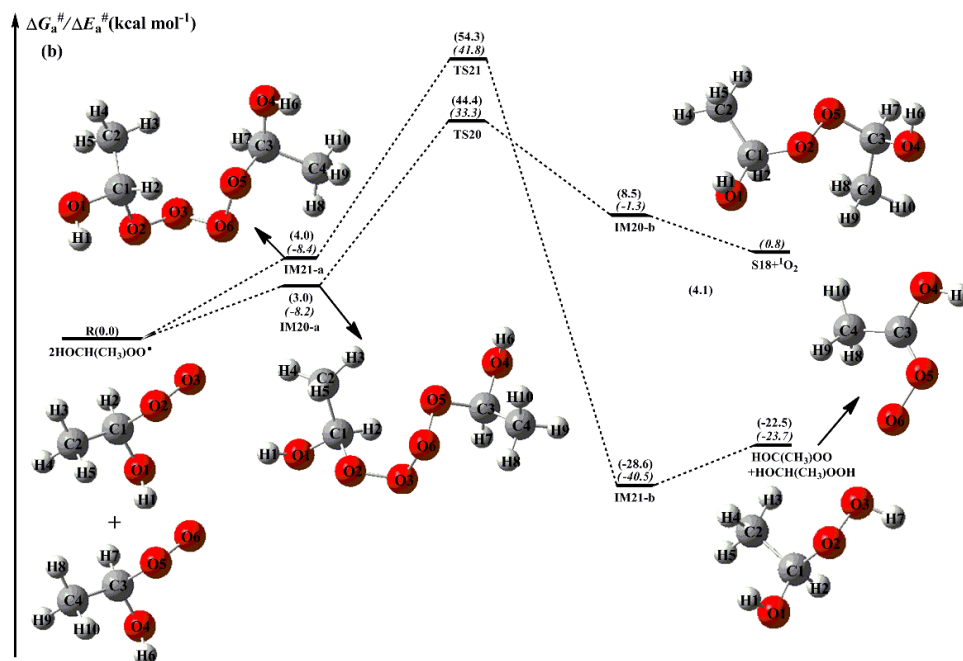
476



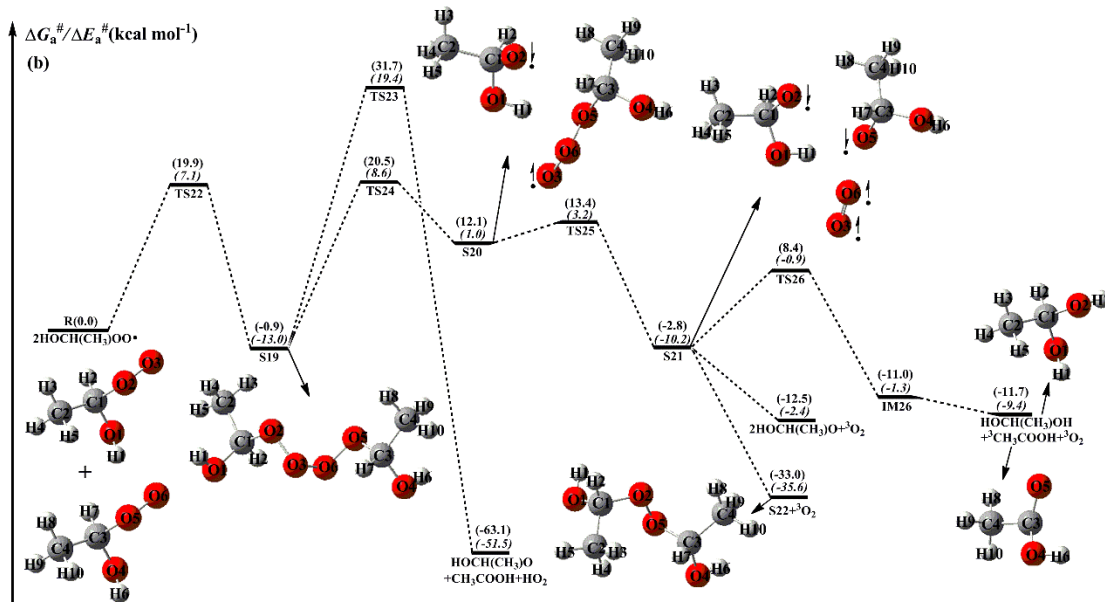
477

478 **Figure 5.** PES ( $\Delta G_a^\#$  and  $\Delta E_a^\#$ , in italics) for the self-reaction of HOCH<sub>2</sub>OO radicals predicted at  
 479 the M06-2X/ma-TZVP//M06-2X/6-311+G(2df,2p) level of theory

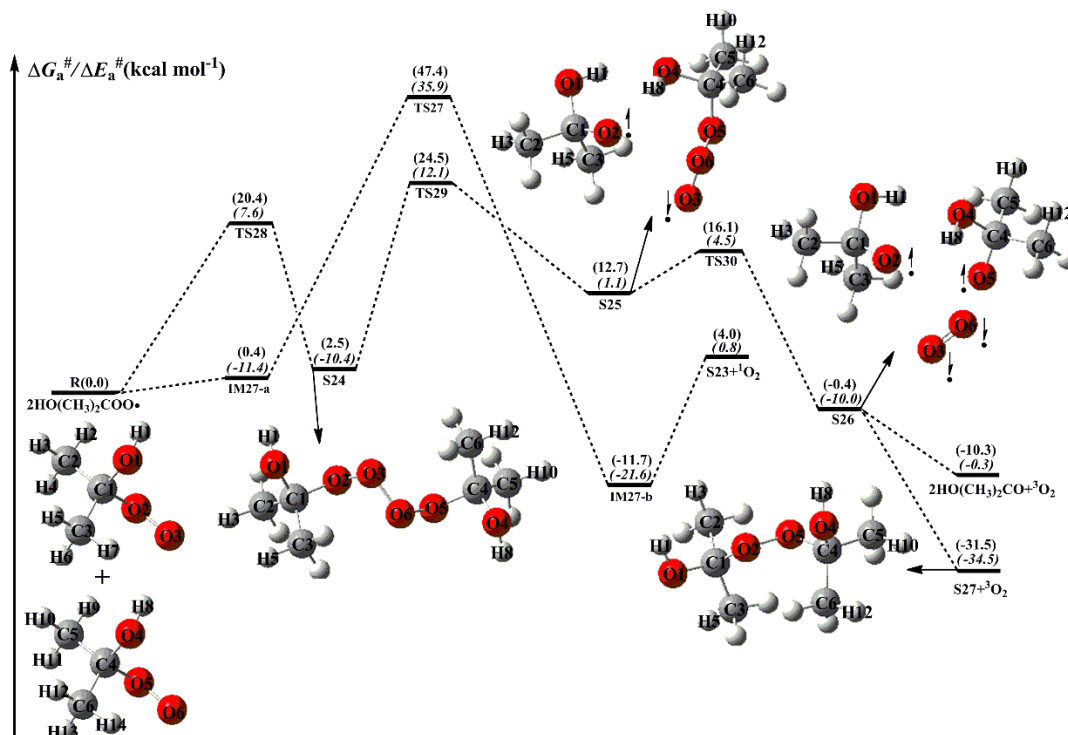
480



481



482 **Figure 6.** PES ( $\Delta G_a^\ddagger$  and  $\Delta E_a^\ddagger$ , in italics) for the self-reaction of HOCH(CH<sub>3</sub>)OO radicals  
 483 predicted at the M06-2X/ma-TZVP//M06-2X/6-311+G(2df,2p) level of theory



484

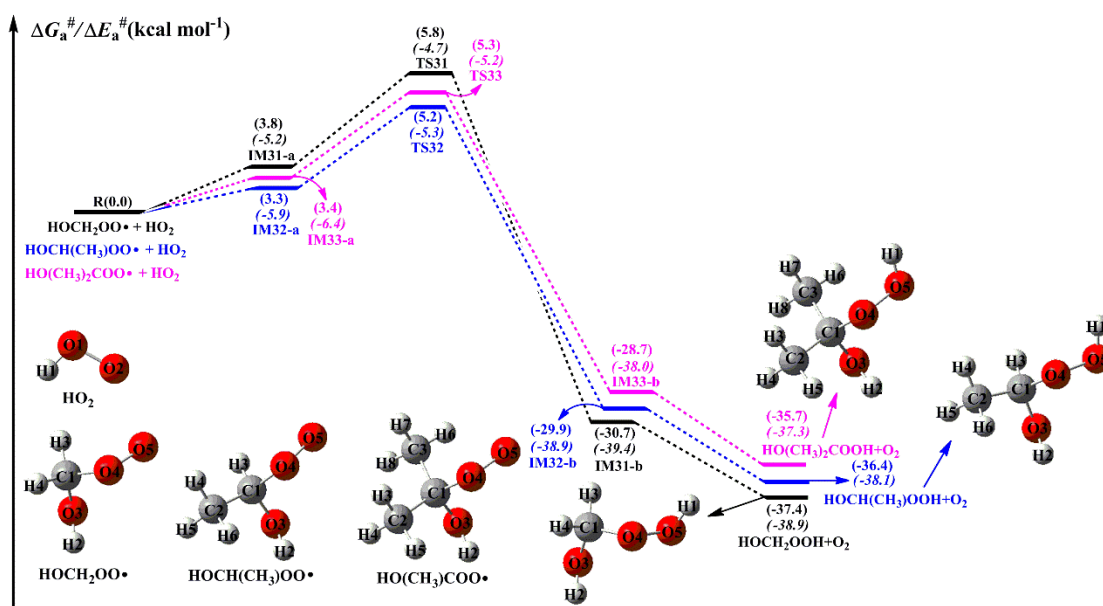
485 **Figure 7.** PES ( $\Delta G_a^\ddagger$  and  $\Delta E_a^\ddagger$ , in italics) for the self-reaction of  $\text{HO}(\text{CH}_2)_2\text{COO}$  radicals  
 486 predicted at the M06-2X/ma-TZVP//M06-2X/6-311+G(2df,2p) level of theory

### 487 3.2.2 Reactions mechanism for the reaction of $\text{RO}_2$ radicals with $\text{HO}_2$ 488 radical

489 When NO is present in low concentration, the bimolecular reaction of  $\text{RO}_2$   
 490 radicals with  $\text{HO}_2$  radical is generally expected to be the dominant pathway as the  
 491 main product hydroperoxide  $\text{ROOH}$ . The **primary** sources of  $\text{HO}_2$  radical involve the  
 492 photo-oxidation of oxygenated volatile organic compounds (OVOCs) and the  
 493 ozonolysis reaction, as well as **secondary** sources include the reactions of OH radical  
 494 with CO, ozone and volatile organic compounds (VOCs), the reaction of alkoxy  
 495 radical RO with  $\text{O}_2$  and the red-light-induced decomposition of  $\alpha$ -hydroxy  
 496 methylperoxy radical  $\text{OHCH}_2\text{OO}$  (Kumar and Francisco, 2015; Stone et al., 2012;  
 497 Hofzumahaus et al., 2009). The atmospheric concentration of  $\text{HO}_2$  radical is  $1.5\text{-}10 \times$   
 498  $10^8$  molecules  $\text{cm}^{-3}$  at ground level in polluted urban environments (Stone et al., 2012).  
 499 A schematic PES for the reactions of distinct  $\text{RO}_2$  radicals with  $\text{HO}_2$  radical is  
 500 presented in Figure 8. As shown in Figure 8, all the reactions are strongly exothermic  
 501 and spontaneous, indicating that they are feasible thermodynamically in the  
 502 atmosphere. The reaction for  $\text{HOCH}_2\text{OO}$  with  $\text{HO}_2$  (R31) starts with the formation of

503 a pre-reactive complex IM31-a in the entrance channel, which is more stable than the  
504 separate reactants by  $3.8 \text{ kcal mol}^{-1}$  in energy. Then it converts into HOCH<sub>2</sub>OOH and  
505 O<sub>2</sub> via a hydrogen atom transfer from the HO<sub>2</sub> radical to the terminal oxygen atom of  
506 HOCH<sub>2</sub>OO radical with the barrier of  $2.0 \text{ kcal mol}^{-1}$ . The mechanism of  
507 HOCH(CH<sub>3</sub>)OO + HO<sub>2</sub> (R32) and HO(CH<sub>3</sub>)<sub>2</sub>COO + HO<sub>2</sub> (R33) reactions is quite  
508 similar to that of HOCH<sub>2</sub>OO + HO<sub>2</sub> system. In order to avoid redundancy, we will not  
509 discuss them in detail. It deserves mentioning that the barrier height is only reduced  
510 by  $0.1 \text{ kcal mol}^{-1}$  when one or two methyl substitutions occur at the C1-position of  
511 HOCH<sub>2</sub>OO radical, compared to the barrier of HOCH<sub>2</sub>OO + HO<sub>2</sub> reaction. This result  
512 implies that the barrier height is not seem to be influenced by the number of methyl  
513 substitution. The rate coefficients of distinct [RO<sub>2</sub> radical reactions](#) with HO<sub>2</sub> radical  
514 are summarized in Table S5 and Figure S12. As shown in Table S5, the rate  
515 coefficients  $k_{R31}$  of HOCH<sub>2</sub>OO + HO<sub>2</sub> reaction vary from  $3.1 \times 10^{-11}$  (273 K) to  $2.1 \times$   
516  $10^{-12} \text{ cm}^3 \text{ molecule}^{-1} \text{ s}^{-1}$  (400 K), and they exhibit a negative temperature dependence.  
517 Similar conclusion is also obtained from the rate coefficients  $k_{R32}$  and  $k_{R33}$  that they  
518 [decrease](#) with the temperature increasing. It should be noted that the rate coefficient is  
519 slightly increased as the number of methyl group is increased. At ambient temperature,  
520  $k_{R31}$  is estimated to be  $1.7 \times 10^{-11} \text{ cm}^3 \text{ molecule}^{-1} \text{ s}^{-1}$ , which is in good agreement with  
521 the value of  $\sim 2 \times 10^{-11} \text{ cm}^3 \text{ molecule}^{-1} \text{ s}^{-1}$  for the reaction of acyl peroxy radicals with  
522 HO<sub>2</sub> radical (Wennberg et al., 2018). The typical atmospheric concentrations of HO<sub>2</sub>  
523 radical are 5, 20 and 50 pptv in the urban, rural and forest environments (Bianchi et  
524 al., 2019), translating into the pseudo-first-order rate constants  $k'_{HO_2} = k_{HO_2}[HO_2]$  of  
525  $1.1 \times 10^{-3}$ ,  $4.2 \times 10^{-3}$  and  $1.1 \times 10^{-2} \text{ s}^{-1}$ , respectively. The pseudo-first-order rate  
526 constants of R32 and R33 are predicted to be  $3.0 \times 10^{-3}$  and  $4.8 \times 10^{-3}$  (urban),  $1.1 \times$   
527  $10^{-2}$  and  $1.8 \times 10^{-2}$  (rural),  $3.0 \times 10^{-2}$  and  $4.8 \times 10^{-2} \text{ s}^{-1}$  (forest) at room temperature.

528



529

530 **Figure 8.** PES ( $\Delta G_a^\ddagger$  and  $\Delta E_a^\ddagger$ , in italics) for the reactions of HO<sub>2</sub> radical with distinct RO<sub>2</sub>  
 531 radicals predicted at the M06-2X/ma-TZVP//M06-2X/6-311+G(2df,2p) level of theory

### 532 3.2.3 Reactions mechanism for the isomerization of RO<sub>2</sub> radicals

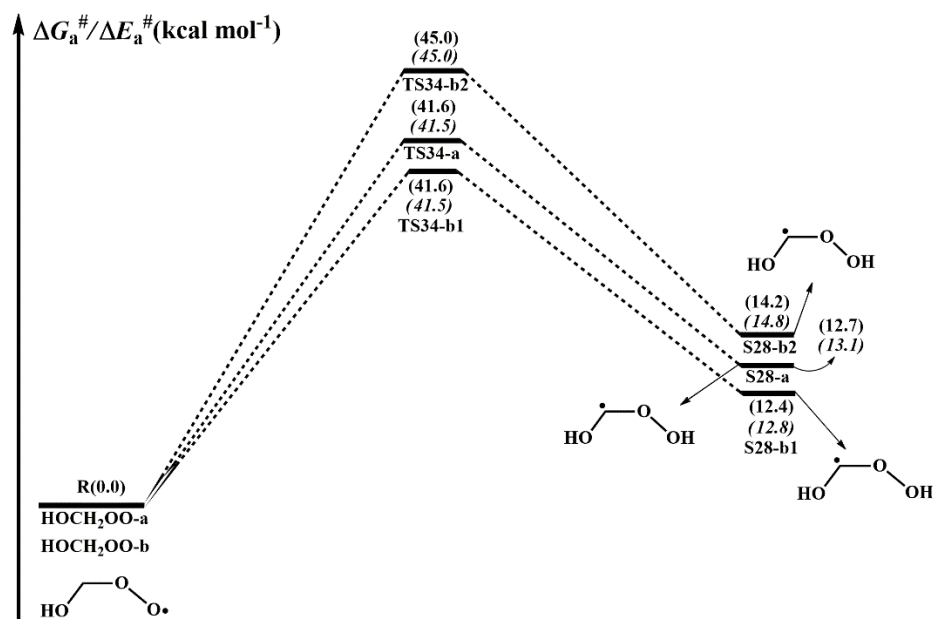
533 Autoxidation of RO<sub>2</sub> radicals is known to play an important role in the  
 534 (re)generation of HO<sub>x</sub> radicals and in the formation of HOMs (Xu et al., 2014;  
 535 Bianchi et al., 2019; Rissanen et al., 2014; Ehn et al., 2017). The autoxidation  
 536 mechanism includes an intramolecular H-shift from the -CH<sub>3</sub> or -CH<sub>2</sub>- groups to the  
 537 -OO site, leading to the formation of a hydroperoxyalkyl radical QOOH, followed by  
 538 O<sub>2</sub> addition to form a new peroxy radical (HOOQO<sub>2</sub>), one after the other, **resulting in**  
 539 **formation of HOMs** (Rissanen et al., 2014; Berndt et al., 2015). For the H-shift  
 540 reactions of RO<sub>2</sub> radicals, reactants, transition states and products have multiple  
 541 conformers due to the effect of degree of freedom for internal rotation. Based on the  
 542 calculated results, it can be found that HOCH<sub>2</sub>OO radical has four energetically  
 543 similar conformers (HOCH<sub>2</sub>OO-a, HOCH<sub>2</sub>OO-b, HOCH<sub>2</sub>OO-c and HOCH<sub>2</sub>OO-d).  
 544 The relative free energy and Boltzmann population ( $w_i$ ) of individual conformer are  
 545 listed in Table S6. As shown in Table S6, the Boltzmann populations of these four  
 546 conformers are 46.39, 46.31, 2.99 and 4.32%, respectively.

547 A schematic PES for the H-shift reaction of HOCH<sub>2</sub>OO radical is displayed in  
 548 Figure 9. As can be seen in Figure 9, the lowest-energy conformer HOCH<sub>2</sub>OO-a can  
 549 proceed via a 1,3-H shift from the -CH<sub>2</sub> group to the terminal oxygen leading to the

550 formation of S28-a (HOCHOOH) with the barrier of 41.6 kcal mol<sup>-1</sup>. HOCH<sub>2</sub>OO-b  
551 can isomerize to S28-b1 and S28-b2 via the four-membered ring transition states  
552 TS34-b1 and TS34-b2 (1,3-H shifts) with the barriers of 41.6 and 45.0 kcal mol<sup>-1</sup>. But  
553 these three 1,3-H shift reactions have comparatively high barriers, making them  
554 irrelevant in the atmosphere. Despite many attempts, the transition states of H-shift  
555 reactions of HOCH<sub>2</sub>OO-c and HOCH<sub>2</sub>OO-d are not located. The result implies that  
556 the H-shift reactions of these two conformers are inhibited, which is consistent with  
557 the previous study that not all reactants will be in a conformation with a path across  
558 the barrier to reaction in the H-shift reactions of RO<sub>2</sub> radicals (Møller et al., 2016).  
559 Equivalent to the case of HOCH<sub>2</sub>OO radical, the isomerization of HOCH(CH<sub>3</sub>)OO  
560 radical proceeds via the 1,3- and 1,4-H shifts from the -CH or -CH<sub>3</sub> groups to the  
561 terminal oxygen resulting in formation of hydroperoxyalkyl radicals (Figure S13).  
562 These 1,3- and 1,4-H shift reactions accompany with the extremely high barriers (>  
563 37.9 kcal mol<sup>-1</sup>), implying that they are of less importance in the atmosphere. Similar  
564 conclusion is also derived from the isomerization of HO(CH<sub>3</sub>)<sub>2</sub>COO radical that 1,4-H  
565 shift reactions are unfavourable kinetically (Figure S14). The high barriers of 1,3- and  
566 1,4-H shifts can be interpreted as the result of the large ring strain energy (RSE) in the  
567 cyclic transition state geometries. As a consequence, the isomerization reactions of  
568 HOCH<sub>2</sub>OO, HOCH(CH<sub>3</sub>)OO and HO(CH<sub>3</sub>)<sub>2</sub>COO radicals are unlikely to proceed in  
569 the atmosphere. [This conclusion is further supported by the previous studies that the  
570 intramolecular H-shift isomerizations are important only for RO<sub>2</sub> radicals with larger  
571 carbon structures \(Crouse et al., 2013; Jokinen et al., 2014; Rissanen et al., 2014\).](#)

572 The single-conformer rate coefficients ( $k_{\text{IRC-TST}}$ ) and multi-conformer rate  
573 coefficients ( $k_{\text{MC-TST}}$ ) of the isomerization of HOCH<sub>2</sub>OO, HOCH(CH<sub>3</sub>)OO and  
574 HOC(CH<sub>3</sub>)<sub>2</sub>OO radicals are calculated over the temperature range of 273-400 K as  
575 listed in Table S9-S11. As can be seen in Table S9,  $k_{\text{IRC-TST}}$  of each conformer exhibits  
576 a marked positive temperature dependence over the temperature range studied.  
577  $k_{\text{MC-TST}}$  is significantly increased with rising temperature, implying that the  
578 temperature increasing is beneficial to the occurrence of HOCH<sub>2</sub>OO radical  
579 isomerization. Similar conclusion is also obtained from the isomerization of

580 HOCH(CH<sub>3</sub>)OO and HOC(CH<sub>3</sub>)<sub>2</sub>OO radicals (Table S10-S11). It is worth mentioning  
 581 that  $k_{\text{MC-TST}}$  is rapidly increased as the number of methyl group is increased. For  
 582 example, the room temperature  $k_{\text{MC-TST}}$  of HOCH<sub>2</sub>OO radical isomerization is  
 583 calculated to be  $4.4 \times 10^{-16} \text{ s}^{-1}$ , which is lower than those of the HOCH(CH<sub>3</sub>)OO ( $2.9$   
 584  $\times 10^{-13} \text{ s}^{-1}$ ) and HO(CH<sub>3</sub>)<sub>2</sub>COO ( $3.0 \times 10^{-12} \text{ s}^{-1}$ ) radicals isomerization by 660 and  
 585 6820 times, respectively.



586  
 587 **Figure 9.** PES ( $\Delta G_a^\ddagger$  and  $\Delta E_a^\ddagger$ , in italics) for the isomerization of HOCH<sub>2</sub>OO radical predicted at  
 588 the M06-2X/ma-TZVP//M06-2X/6-311+G(2df,2p) level of theory

### 589 3.3 Subsequent reactions of H-abstraction products RO<sub>2</sub> radicals 590 in urban environments

591 NO<sub>x</sub> is present in high concentration in urban environments, reaction with NO is  
 592 the dominant chemical sink for RO<sub>2</sub> radicals (Atkinson and Arey, 2003; Orlando and  
 593 Tyndall, 2012; Perring et al., 2013). The main pathways in this type of reaction lead to  
 594 the formations of NO<sub>2</sub>, RO radicals, organic nitrites, and organic nitrates, and their  
 595 formation yields are highly dependent on the nature of R group (Orlando and Tyndall,  
 596 2012). The formation of NO<sub>2</sub> through subsequent photolysis ( $\lambda < 420 \text{ nm}$ ) produces  
 597 ozone and NO, increasing the concentrations of near-surface ozone and propagating  
 598 NO<sub>x</sub> chain (Orlando and Tyndall, 2012). The schematic PES for the reactions of  
 599 distinct RO<sub>2</sub> radicals with NO are displayed in Figures 10-12. As shown in Figure 10,  
 600 the bimolecular reaction of HOCH<sub>2</sub>OO radical with NO initially leads to nitrite adduct

601 S31 via the barrierless addition of NO to terminal oxygen atom O<sub>3</sub> of HOCH<sub>2</sub>OO  
602 radical. The formed S31 exists two isomers: S31-*cis* refers to the O<sub>2</sub> and O<sub>4</sub> on the  
603 same side ( $\text{DO}_2\text{O}_3\text{N}_1\text{O}_4 = 2.3^\circ$ ), whereas S31-*trans* refers to the O<sub>2</sub> and O<sub>4</sub> on the  
604 opposite side ( $\text{DO}_2\text{O}_3\text{N}_1\text{O}_4 = -179.8^\circ$ ) with respect to the O<sub>3</sub>-N<sub>1</sub> bond. The  
605 calculations show that S31-*cis* is more stable than S31-*trans* by 1.1 kcal mol<sup>-1</sup> in  
606 energy. The tautomerization between S31-*cis* and S31-*trans* proceeds through the  
607 rotating of O<sub>3</sub>-N<sub>1</sub> bond with the barrier of 14.4 kcal mol<sup>-1</sup>, implying that they can be  
608 regarded as the separate atmospheric species. According to the Boltzmann-weighted  
609 distribution, at room temperature, the predicted percentages of S31-*cis* and S31-*trans*  
610 are 86.5% and 13.5%, respectively. The result implies that the dominant product of  
611 HOCH<sub>2</sub>OO radical reaction with NO is S31-*cis*, and it is selected as a model  
612 compound to insight into the mechanism of secondary reactions in the following  
613 sections.

614 S31-*cis* can either isomerize to organic nitrate S32 (R38) via a concerted  
615 process of O<sub>2</sub>-O<sub>3</sub> bond breaking and O<sub>2</sub>-N<sub>1</sub> bond forming with the barrier of 47.8  
616 kcal mol<sup>-1</sup>, or decompose into HOCH<sub>2</sub>O radical and NO<sub>2</sub> (R39) via the cleavage of  
617 O<sub>2</sub>-O<sub>3</sub> bond with the barrier of 11.3 kcal mol<sup>-1</sup>. The result shows that the latter  
618 pathway is more favourable than the former channel. Similar conclusion is also  
619 obtained from the reactions of NO with HOCH(CH<sub>3</sub>)OO and HO(CH<sub>3</sub>)<sub>2</sub>COO radicals  
620 that the formation of organic nitrate is of minor importance in the atmosphere. This  
621 result is further supported by the prior studies that the direct formation of organic  
622 nitrate from peroxy nitrites is a minor channel in the reactions of isoprene-derived  
623 RO<sub>2</sub> radicals with NO (Piletic et al., 2017; Zhang et al., 2002). It should be noted that  
624 the transition state TS39 is not located using M06-2X functional, but it is located at  
625 the MP2/6-311+G(2df,2p) level of theory and is verified using IRC calculations. The  
626 formed HOCH<sub>2</sub>O radical has two possible pathways: (1) it directly decomposes into  
627 CH<sub>2</sub>O and OH radical (R40) via  $\beta$ -site C<sub>1</sub>-O<sub>1</sub> bond scission with the barrier of 52.4  
628 kcal mol<sup>-1</sup>; (2) it converts into HCOOH and HO<sub>2</sub> radical (R41) through H-abstraction  
629 by O<sub>2</sub> with the barrier of 26.4 kcal mol<sup>-1</sup>. This result reveals that R41 is the most  
630 feasible channel in the fragmentation of HOCH<sub>2</sub>O radical.

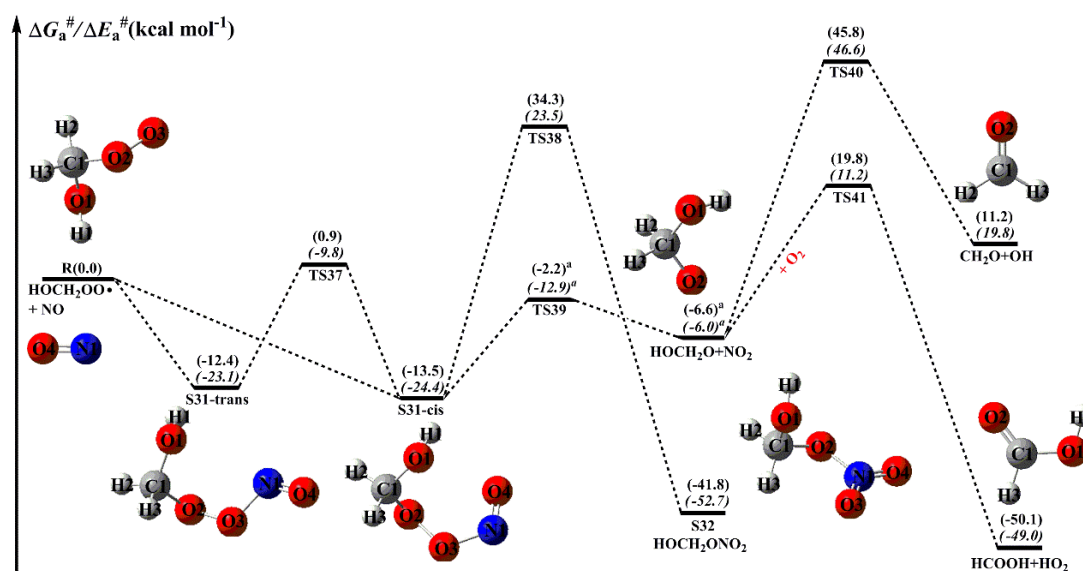
631 From Figure 11, it can be seen that the addition NO to HOCH(CH<sub>3</sub>)OO radical  
632 leading to the formation of S33-*cis* is barrierless. Then, it decomposes into  
633 HOCH(CH<sub>3</sub>)O radical and NO<sub>2</sub> (R44) via the cleavage of O<sub>2</sub>-O<sub>3</sub> bond with the barrier  
634 of 11.5 kcal mol<sup>-1</sup>. The resulting HOCH(CH<sub>3</sub>)O radical has three possible pathways.  
635 The first one is  $\beta$ -site C<sub>1</sub>-C<sub>2</sub> bond scission leading to the formation of HCOOH + CH<sub>3</sub>  
636 (R45) with the barrier of 8.3 kcal mol<sup>-1</sup>. The second one is  $\beta$ -site C<sub>1</sub>-O<sub>1</sub> bond cleavage  
637 resulting in formation of CH<sub>3</sub>COH + OH (R46) with the barrier of 26.7 kcal mol<sup>-1</sup>.  
638 The third one is H-abstraction by O<sub>2</sub> leading to CH<sub>3</sub>COOH + HO<sub>2</sub> (R47) with the  
639 barrier of 26.2 kcal mol<sup>-1</sup>. Based on the calculated reaction barriers, it can be found  
640 that  $\beta$ -site C<sub>1</sub>-C<sub>2</sub> bond scission is the dominant pathway in the fragmentation of  
641 HOCH(CH<sub>3</sub>)O radical. This conclusion is further supported by the previous  
642 experimental result that  $\beta$ -hydroxy intermediates primarily proceed decomposition  
643 rather than react with O<sub>2</sub> in the presence of NO (Aschmann et al., 2000). Equivalent to  
644 the HOCH(CH<sub>3</sub>)OO + NO reaction, the bimolecular reaction of HO(CH<sub>3</sub>)<sub>2</sub>COO  
645 radical with NO has similar transformation pathways (Figure 12). The reaction for  
646 HO(CH<sub>3</sub>)<sub>2</sub>COO with NO initially proceeds via a barrierless addition leading to  
647 S35-*cis* with the binding energy of 12.6 kcal mol<sup>-1</sup>. Then, S35-*cis* fragments into  
648 HO(CH<sub>3</sub>)<sub>2</sub>CO radical along with NO<sub>2</sub> (R50) via the cleavage of O<sub>2</sub>-O<sub>3</sub> bond with the  
649 barrier of 11.4 kcal mol<sup>-1</sup>. The formed HO(CH<sub>3</sub>)<sub>2</sub>CO radical can either dissociate to  
650 CH<sub>3</sub>COOH + CH<sub>3</sub> (R51) via the C<sub>1</sub>-C<sub>3</sub> bond scission with the barrier of 8.2 kcal mol<sup>-1</sup>,  
651 or decompose into CH<sub>3</sub>COCH<sub>3</sub> + OH (R52) through the C<sub>1</sub>-O<sub>1</sub> bond breaking with the  
652 barrier of 24.3 kcal mol<sup>-1</sup>. The result again shows that the  $\beta$ -site C-C bond scission is  
653 the **dominant** pathway.

654 The typical atmospheric concentrations of NO are about 10 ppbv, 1 ppbv and 20  
655 pptv in the urban, rural and forest environments (Bianchi et al., 2019). The rate  
656 coefficient of HOCH<sub>2</sub>OO radical reaction with NO is calculated to be  $4.3 \times 10^{-12}$  cm<sup>3</sup>  
657 molecule<sup>-1</sup> s<sup>-1</sup> at room temperature, resulting in the pseudo-first-order rate constants  
658  $k'_{\text{NO}} = k_{\text{NO}}[\text{NO}]$  of  $6.5 \times 10^{-1}$ ,  $6.5 \times 10^{-2}$ , and  $1.3 \times 10^{-3}$ , respectively, in the urban,  
659 rural and forest environments. It is of interest to assess the relative importance for the  
660 H-shift reaction of HOCH<sub>2</sub>OO radical and bimolecular reactions with HO<sub>2</sub> radical and

661 NO based on the calculated  $k_{\text{MC-TST}}$ ,  $k'_{\text{HO}_2}$  and  $k'_{\text{NO}}$ . It can be found that the H-shift  
 662 reaction is of less importance, the  $\text{HO}_2$  radical reaction is favorable in the forest  
 663 environments, while the NO reaction is predominant in the urban and rural regions.  
 664 Similar conclusion is also obtained from the cases of  $\text{HOCH}(\text{CH}_3)\text{OO}$  and  
 665  $\text{HO}(\text{CH}_3)_2\text{CHOO}$  radicals.

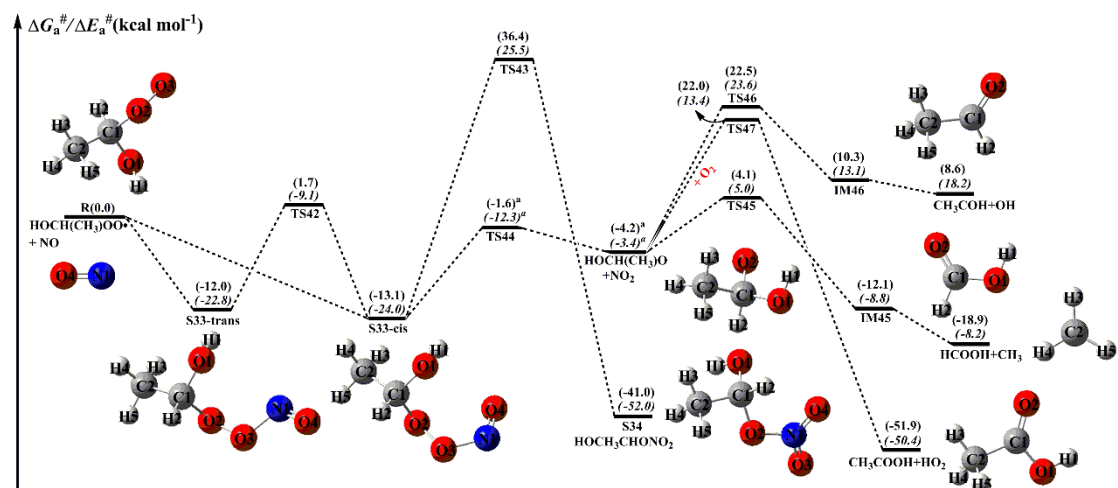
666 The rate coefficients of the dominant pathways of  $\text{HOCH}_2\text{O}$ ,  $\text{HOCH}(\text{CH}_3)\text{O}$  and  
 667  $\text{HO}(\text{CH}_3)_2\text{CHO}$  radicals fragmentation are summarized in Table S12. As can be seen  
 668 in Table S12,  $k_{\text{R41}}$  is slightly increased with the temperature increasing, and the  
 669 discrepancy is about a factor of 12 at the two extremes of temperature. At ground  
 670 level with  $[\text{O}_2] \sim 5.0 \times 10^{18}$  molecule  $\text{cm}^{-3}$ , the pseudo-first-order rate constant  $k'_{\text{O}_2}$   
 671  $= k_{\text{R41}}[\text{O}_2]$  is estimated to be  $38.0 \text{ s}^{-1}$  at room temperature.  $k_{\text{R45}}$  vary significantly from  
 672  $2.0 \times 10^6$  (273 K) to  $3.1 \times 10^8$  (400 K)  $\text{s}^{-1}$ , and they exhibit a marked positive  
 673 temperature dependence. Similar phenomenon is also observed from  $k_{\text{R51}}$  that  $k_{\text{R51}}$  is  
 674 significantly increased with increasing temperature.  $k_{\text{R51}}$  is a factor of  $\sim 1.3$  greater  
 675 than  $k_{\text{R45}}$  in the temperature range studied, implying that the rate coefficient of  $\beta$ -site  
 676 C-C bond scission is slightly increased as the number of methyl group is increased.

677



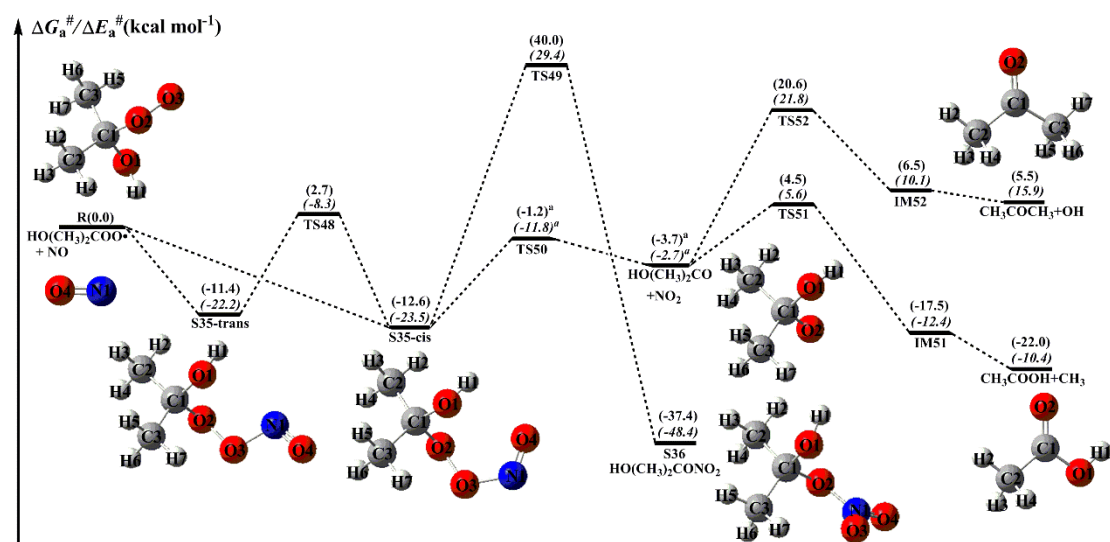
678

679 **Figure 10.** PES ( $\Delta G_a^\ddagger$  and  $\Delta E_a^\ddagger$ , in italics) for the reaction of  $\text{HOCH}_2\text{OO}$  radical with NO  
 680 predicted at the M06-2X/ma-TZVP//M06-2X/6-311+G(2df,2p) level of theory (the superscript a is  
 681 calculated at the MP2/ma-TZVP//MP2/6-311+G(2df,2p) level)



682

683 **Figure 11.** PES ( $\Delta G_a^\ddagger$  and  $\Delta E_a^\ddagger$ , in italics) for the reaction of HOCH(CH<sub>3</sub>)OO radical with NO  
 684 predicted at the M06-2X/ma-TZVP//M06-2X/6-311+G(2df,2p) level of theory (the superscript a is  
 685 calculated at the MP2/ma-TZVP//MP2/6-311+G(2df,2p) level)



686

687 **Figure 12.** PES ( $\Delta G_a^\ddagger$  and  $\Delta E_a^\ddagger$ , in italics) for the reaction of HO(CH<sub>3</sub>)<sub>2</sub>COO radical with NO  
 688 predicted at the M06-2X/ma-TZVP//M06-2X/6-311+G(2df,2p) level of theory (the superscript a is  
 689 calculated at the MP2/ma-TZVP//MP2/6-311+G(2df,2p) level)

## 690 4. Conclusions

691 The detailed mechanisms and kinetic properties of OH-initiated oxidation of  
 692 distinct HHPs and subsequent transformation of resulting H-abstraction products are  
 693 investigated using quantum chemical and kinetics modeling methods. The main  
 694 conclusions are summarized as follows:

- 695 (a) The dominant pathway is the H-abstraction from the -OOH group in the  
 696 initiation reactions of OH radical with HOCH<sub>2</sub>OOH and HOC(CH<sub>3</sub>)<sub>2</sub>OOH.  
 697 H-abstraction from the -CH group is competitive with that from the -OOH group in

698 the reaction of OH radical with HOCH(CH<sub>3</sub>)OOH. The barrier of H-abstraction from  
699 the -OOH group is slightly increased as the number of methyl group is increased.  
700 Compared with the rate coefficient of dominant pathway in the parent system, it is  
701 almost identical when a methyl group substitution occurs at the C<sub>1</sub>-position, whereas  
702 it reduces by a factor of 2-5 when two methyl groups are introduced into the  
703 C<sub>1</sub>-position. The atmospheric lifetime of HOCH<sub>2</sub>OOH, HOCH(CH<sub>3</sub>)OOH and  
704 HO(CH<sub>3</sub>)<sub>2</sub>OOH reactivity toward OH radical are estimated to be 0.58-1.74 h,  
705 0.60-1.79 h and 1.23-3.69 h at room temperature under the typical OH radical  
706 concentrations of  $5-15 \times 10^6$  molecules cm<sup>-3</sup> during daylight.

707 (b) The self-reaction of H-abstraction product RO<sub>2</sub> radical initially produces  
708 tetroxide intermediate via an oxygen-to-oxygen coupling, then it decomposes into  
709 propagation and termination products through the asymmetric two-step O-O bond  
710 scission. The rate-limiting step is the first O-O bond cleavage, and the barrier is  
711 increased with increasing the number of methyl group. This finding is meaningful to  
712 understand the self-reaction of complex RO<sub>2</sub> radicals.

713 (c) The bimolecular reactions of distinct RO<sub>2</sub> radicals with HO<sub>2</sub> radical lead to  
714 the formation of hydroperoxide ROOH as the main product, and the barrier height is  
715 independent on the number of methyl substitution. When compared to the rate  
716 coefficient for HOCH<sub>2</sub>OO + HO<sub>2</sub> reaction, the rate coefficients increase by a factor of  
717 2-5 when one or two methyl groups are introduced into the C<sub>1</sub>-position. Using a HO<sub>2</sub>  
718 radical concentration of ~50 pptv in the forest environments, the pseudo-first-order  
719 rate constants  $k'_{\text{HO}_2}$  of distinct RO<sub>2</sub> radical reactions with HO<sub>2</sub> radical vary from 1 to  $5$   
720  $\times 10^{-2}$  s<sup>-1</sup>.

721 (d) The isomerization reactions of HOCH<sub>2</sub>OO, HOCH(CH<sub>3</sub>)OO and  
722 HO(CH<sub>3</sub>)<sub>2</sub>COO radicals are unlikely to proceed in the atmosphere because the  
723 intramolecular H-shift steps have dramatically high barriers and strongly endergonic.  
724 The result implies that the isomerization of RO<sub>2</sub> radicals with smaller carbon  
725 structures is of less importance in the atmosphere.

726 (e) Reaction with O<sub>2</sub> forming formic acid and HO<sub>2</sub> radical is the dominant  
727 removal pathway for HOCH<sub>2</sub>O radical formed from the reaction of HOCH<sub>2</sub>OO

728 radical with NO. The  $\beta$ -site C-C bond scission is the **dominant** pathway in the  
729 dissociation of HOCH(CH<sub>3</sub>)O and HOC(CH<sub>3</sub>)<sub>2</sub>O radicals formed from **the reactions**  
730 **of NO with HOCH(CH<sub>3</sub>)OO and HOC(CH<sub>3</sub>)<sub>2</sub>OO radicals.** The result implies that the  
731 **methyl-substituted alkoxy radicals primarily proceed via  $\beta$ -site C-C bond scission to**  
732 **produce aldehyde rather than react with O<sub>2</sub>.**

733

## 734 **Data availability**

735 The data are accessible by contacting the corresponding author  
736 (huangyu@ieecas.cn).

## 737 **Supplement**

738 The following information is provided in the Supplement: Y//X (Y = M06-2X,  
739 CCSD(T), X = 6-311+G(2df,2p), ma-TZVP) calculated energy barrier ( $\Delta E_a^\#$ ,  $\Delta G_a^\#$ )  
740 for OH + HHPs reactions; Rate coefficients of every elementary pathway involved in  
741 the initial reactions of OH radical with HOCH<sub>2</sub>OOH, HOCH(CH<sub>3</sub>)OOH and  
742 HO(CH<sub>3</sub>)<sub>2</sub>COOH; Rate coefficients of HO<sub>2</sub> radical reactions with HOCH<sub>2</sub>OO,  
743 HOCH(CH<sub>3</sub>)OO and HO(CH<sub>3</sub>)<sub>2</sub>COO radicals; The relative free energy and  
744 Boltzmann populations ( $w_i$ ) of the conformer of HOCH<sub>2</sub>OO, HOCH(CH<sub>3</sub>)OO and  
745 HO(CH<sub>3</sub>)<sub>2</sub>COO radicals; The single-conformer rate coefficients ( $k_{\text{IRC-TST}}$ ) and  
746 multi-conformer rate coefficients ( $k_{\text{MC-TST}}$ ) of HOCH<sub>2</sub>OO, HOCH(CH<sub>3</sub>)OO and  
747 HO(CH<sub>3</sub>)<sub>2</sub>COO radicals; Rate coefficients of dominant pathways in the HOCH<sub>2</sub>OO · +  
748 NO, HOCH(CH<sub>3</sub>)OO · + NO and HO(CH<sub>3</sub>)<sub>2</sub>CHOO · + NO reactions; PESs ( $\Delta E_a^\#$ ) for  
749 the OH-initiated reactions of HOCH<sub>2</sub>OOH, HOCH(CH<sub>3</sub>)OOH, HOC(CH<sub>3</sub>)<sub>2</sub>OOH;  
750 Geometries of all the stationary points; Plots of the rate coefficients of every  
751 elementary pathway versus temperature; PESs ( $\Delta G_a^\#$  and  $\Delta E_a^\#$ , in italics) for the  
752 isomerization of HOCH(CH<sub>3</sub>)OO and HO(CH<sub>3</sub>)<sub>2</sub>COO radicals.

753

## 754 **Author contribution**

755 LC designed the study. LC and YH wrote the paper. LC performed theoretical

756 calculation. YX, ZJ, and WW analyzed the data. All authors reviewed and commented  
757 on the paper.

758

## 759 **Competing interests**

760 The authors declare that they have no conflict of interest.

761

## 762 **Acknowledgments**

763 This work was supported by the National Natural Science Foundation of China  
764 (grant Nos. 42175134, 41805107, and 22002080). It was also partially supported as  
765 Key Projects of Chinese Academy of Sciences, China (grant No. ZDRW-ZS-2017-6),  
766 Strategic Priority Research Program of the Chinese Academy of Sciences, China  
767 (grant Nos. XDA23010300 and XDA23010000), Key Project of International  
768 Cooperation of the Chinese Academy of Sciences, China (grant No. GJHZ1543),  
769 Research Grants Council of Hong Kong, China (grant No. PolyU 152083/14E), CAS  
770 "Light of West China" Program (XAB2019B01) and the General Project of Shaanxi  
771 Province (2020JQ-432).

772

## 773 **References**

- 774 Allen, H. M., Crouse, J. D., Bates, K. H., Teng, A. P., Krawiec-Thayer, M. P., Rivera-Rios, J. C.,  
775 Keutsch, F. N., Clair, J. M. S., Hanisco, T. F., Møller, K. H., Kjaergaard, H. G., and Wennberg,  
776 P. O.: Kinetics and product yields of the OH initiated oxidation of hydroxymethyl  
777 hydroperoxide, *J. Phys. Chem. A*, 122, 6292-6302, <https://doi.org/10.1021/acs.jpca.8b04577>,  
778 2018.
- 779 Anglada, J. M., and Solé A.: Impact of the water dimer on the atmospheric reactivity of carbonyl  
780 oxides, *Phys. Chem. Chem. Phys.*, 18, 17698-17712, <https://doi.org/10.1039/C6CP02531E>,  
781 2016.
- 782 Anglada, J. M., González, J., and Torrent-Sucarrat, M.: Effects of the substituents on the reactivity  
783 of carbonyl oxides. a theoretical study on the reaction of substituted carbonyl oxides with  
784 water, *Phys. Chem. Chem. Phys.*, 13, 13034-13045, <https://doi.org/10.1039/c1cp20872a>,  
785 2011.
- 786 Aschmann, S. M., Arey, J., and Atkinson, R.: Formation of  $\beta$ -hydroxycarbonyls from the OH  
787 radical-initiated reactions of selected alkenes, *Environ. Sci. Technol.*, 34, 1702-1706,  
788 <https://doi.org/10.1021/es991125a>, 2000.

789 Atkinson, R., and Arey, J.: Atmospheric degradation of volatile organic compounds, Chem. Rev.,  
790 103, 4605-4638, <https://doi.org/10.1021/cr0206420>, 2003.

791 Bach, R. D., Dmitrenko, O., and Estévez, C. M.: Chemical behavior of the biradicaloid  
792 (HO ··ONO) singlet states of peroxyoxynitrous acid. the oxidation of hydrocarbons, sulfides, and  
793 selenides, J. Am. Chem. Soc., 127, 3140-3155, <https://doi.org/10.1021/ja044245d>, 2005.

794 Berndt, T., Richters, S., Kaethner, R., Voigtländer, J., Stratmann, F., Sipilä M., Kulmala, M., and  
795 Herrmann, H.: Gas-phase ozonolysis of cycloalkenes: formation of highly oxidized RO<sub>2</sub> radicals  
796 and their reactions with NO, NO<sub>2</sub>, SO<sub>2</sub>, and Other RO<sub>2</sub> radicals, J. Phys. Chem. A, 119,  
797 10336-10348, <https://doi.org/10.1021/acs.jpca.5b07295>, 2015.

798 Berndt, T., Scholz, W., Mentler, B., Fischer, L., Herrmann, H., Kulmala, M., and Hansel, A.:  
799 Accretion product formation from self- and cross-reactions of RO<sub>2</sub> radicals in the atmosphere,  
800 Angew. Chem. Int. Ed., 57, 3820-3824, <https://doi.org/10.1002/anie.201710989>, 2018.

801 Bianchi, F., Kurten, T., Riva, M., Mohr, C., Rissanen, M. P., Roldin, P., Berndt, T., Crouse, J. D.,  
802 Wennberg, P. O., Mentel, T. F., Wildt, J., Junninen, H., Jokinen, T., Kulmala, M., Worsnop, D.  
803 R., Thornton, J. A., Donahue, N., Kjaergaard, H. G., and Ehn, M.: Highly oxygenated organic  
804 molecules (HOM) from gas-phase autoxidation involving peroxy radicals: a key contributor  
805 to atmospheric aerosol, Chem. Rev., 119, 3472-3509,  
806 <https://doi.org/10.1021/acs.chemrev.8b00395>, 2019.

807 Boys, S. F., and Bernardi, F.: The calculation of small molecular interactions by the differences of  
808 separate total energies. Some procedures with reduced errors, Mol. Phys., 19, 553-566,  
809 <https://doi.org/10.1080/00268977000101561>, 1970.

810 Chao, W., Hsieh, J. T., Chang, C. H., and Lin, J. J. M.: Direct kinetic measurement of the reaction  
811 of the simplest Criegee intermediate with water vapor, Science, 347, 751-754,  
812 <https://doi.org/10.1126/science.1261549>, 2015.

813 Chen, L., Huang, Y., Xue, Y., Cao, J., and Wang, W.: Competition between HO<sub>2</sub> and H<sub>2</sub>O<sub>2</sub>  
814 reactions with CH<sub>2</sub>OO/*anti*-CH<sub>3</sub>CHOO in the oligomer formation: a theoretical perspective, J.  
815 Phys. Chem. A, 121, 6981-6991, <https://doi.org/10.1021/acs.jpca.7b05951>, 2017.

816 Chen, L., Huang, Y., Xue, Y., Jia, Z., and Wang, W.: Atmospheric oxidation of 1-butene initiated  
817 by OH radical: Implications for ozone and nitrous acid formations, Atmos. Environ., 244,  
818 118010-118021, <https://doi.org/10.1016/j.atmosenv.2020.118010>, 2021.

819 Chen, L., Huang, Y., Xue, Y., Shen, Z., Cao, J., and Wang, W.: Mechanistic and kinetics  
820 investigations of oligomer formation from Criegee intermediate reactions with hydroxyalkyl  
821 hydroperoxides, Atmos. Chem. Phys., 19, 4075-4091,  
822 <https://doi.org/10.5194/acp-19-4075-2019>, 2019.

823 Chen, L., Wang, W., Wang, W., Liu, Y., Liu, F., Liu, N., and Wang, B.: Water-catalyzed  
824 decomposition of the simplest Criegee intermediate CH<sub>2</sub>OO, Theor. Chem. Acc., 135,  
825 131-143, <https://doi.org/10.1007/s00214-016-1894-9>, 2016b.

826 Chen, L., Wang, W., Zhou, L., Wang, W., Liu, F., Li, C., and Lü, J.: Role of water clusters in the  
827 reaction of the simplest Criegee intermediate CH<sub>2</sub>OO with water vapour, Theor. Chem. Acc.,  
828 135, 252-263, <https://doi.org/10.1007/s00214-016-1998-2>, 2016a.

829 Chhantyal-Pun, R., Welz, O., Savee, J. D., Eskola, A. J., Lee, E. P. F., Blacker, L., Hill, H. R.,  
830 Ashcroft, M., Khan, M. A. H., Lloyd-Jones, G. C., Evans, L., Rotavera, B., Huang, H.,  
831 Osborn, D. L., Mok, D. K. W., Dyke, J. M., Shallcross, D. E., Percival, C. J., Orr-Ewing, A. J.,  
832 and Taatjes, C. A.: Direct measurements of unimolecular and bimolecular reaction kinetics of

833 the Criegee intermediate  $(\text{CH}_3)_2\text{COO}$ , *J. Phys. Chem. A*, 121, 4-15,  
834 <https://doi.org/10.1021/acs.jpca.6b07810>, 2017.

835 Crounse, J. D., Nielsen, L. B., Jørgensen, S., Kjaergaard, H. G., and Wennberg, P. O.:  
836 Autoxidation of organic compounds in the atmosphere, *J. Phys. Chem. Lett.*, 4, 3513-3520,  
837 <https://doi.org/10.1021/jz4019207>, 2013.

838 Dillon, T. J., and Crowley, J. N.: Direct detection of OH formation in the reactions of  $\text{HO}_2$  with  
839  $\text{CH}_3\text{C}(\text{O})\text{O}_2$  and other substituted peroxy radicals, *Atmos. Chem. Phys.*, 8, 4877-4889,  
840 <https://doi.org/10.5194/acp-8-4877-2008>, 2008.

841 Eckart, C.: The penetration of a potential barrier by electrons, *Phys. Rev.*, 35, 1303-1309,  
842 <https://doi.org/10.1103/PhysRev.35.1303>, 1930.

843 Ehn, M., Berndt, T., Wildt, J., and Mentel, T.: Highly oxygenated molecules from atmospheric  
844 autoxidation of hydrocarbons: a prominent challenge for chemical kinetics studies, *Int. J.*  
845 *Chem. Kinet.*, 49, 821-831, <https://doi.org/10.1002/kin.21130>, 2017.

846 Ehn, M., Thornton, J. A., Kleist, E., Sipilä M., Junninen, H., Pullinen, I., Springer, M., Rubach, F.,  
847 Tillmann, R., Lee, B., Lopez-Hilfiker, F., Andres, S., Acir, I. H., Rissanen, M., Jokinen, T.,  
848 Schobesberger, S., Kangasluoma, J., Kontkanen, J., Nieminen, T., Kurtén, T., Nielsen, L. B.,  
849 Jørgensen, S., Kjaergaard, H. G., Canagaratna, M., Maso, M. D., Berndt, T., Petäjä T.,  
850 Wahner, A., Kerminen, V. M., Kulmala, M., Worsnop, D. R., Wildt, J., and Mentel T. F.: A  
851 large source of low-volatility secondary organic aerosol, *Nature*, 506, 476-479,  
852 <https://doi.org/10.1038/nature13032>, 2014.

853 Fernández-Ramos, A., Ellingson, B. A., Meana-Pañeda, R., Marques, J. M. C., and Truhlar, D. G.:  
854 Symmetry numbers and chemical reaction rates, *Theor. Chem. Acc.*, 118, 813-826,  
855 <https://doi.org/10.1007/s00214-007-0328-0>, 2007.

856 Francisco, J. S., and Eisfeld, W.: Atmospheric oxidation mechanism of hydroxymethyl  
857 hydroperoxide, *J. Phys. Chem. A*, 113, 7593-7600, <https://doi.org/10.1021/jp901735z>, 2009.

858 Frisch, M. J., Trucks, G. W., Schlegel, H. B., Scuseria, G. E., Robb, M. A., Cheeseman, J. R.,  
859 Montgomery, J. A. Jr., Vreven, T., Kudin, K. N., Burant, J. C., Millam, J. M., Iyengar, S. S.,  
860 Tomasi, J., Barone, V., Mennucci, B., Cossi, M., Scalmani, G., Rega, N., Petersson, G. A.,  
861 Nakatsuji, H., Hada, M., Ehara, M., Toyota, K., Fukuda, R., Hasegawa, J., Ishida, M.,  
862 Nakajima, T., Honda, Y., Kitao, O., Nakai, H., Klene, M., Li, X., Knox, J. E., Hratchian, H. P.,  
863 Cross, J. B., Adamo, C., Jaramillo, J., Gomperts, R., Stratmann, R. E., Yazyev, O., Austin, A.  
864 J., Cammi, R., Pomelli, C., Ochterski, J. W., Ayala, P. Y., Morokuma, K., Voth, G. A.,  
865 Salvador, P., Dannenberg, J. J., Zakrzewski, V. G., Dapprich, S., Daniels, A. D., Strain, M. C.,  
866 Farkas, O., Malick, D. K., Rabuck, A. D., Raghavachari, K., Foresman, J. B., Ortiz, J. V., Cui,  
867 Q., Baboul, A. G., Clifford, S., Cioslowski, J., Stefanov, B. B., Liu, G., Liashenko, A.,  
868 Piskorz, P., Komaromi, I., Martin, R. L., Fox, D. J., Keith, T., Al-Laham, M. A., Peng, C. Y.,  
869 Nanayakkara, A., Challacombe, M., Gill, P. M. W., Johnson, B., Chen, W., Wong, M. W.,  
870 Gonzalez, C., and Pople, J. A.: Gaussian 09, Revision D.01; Gaussian, Inc.: Wallingford, CT,  
871 2009.

872 Fukui, K.: The path of chemical reactions - the IRC approach, *Acc. Chem. Res.*, 14, 363-368,  
873 <https://doi.org/10.1021/ar00072a001>, 1981.

874 Gilbert, R. G., and Smith, S. C.: Theory of unimolecular and recombination reactions; Blackwell  
875 Scientific: Carlton, Australia, 1990.

876 Gligorovski, S., Strekowski, R., Barbati, S., and Vione, D.: Environmental implications of

877 hydroxyl radicals ( OH), *Chem. Rev.*, 115, 13051-13092, <https://doi.org/10.1021/cr500310b>,  
878 2015.

879 Glowacki, D. R., Liang, C. H., Morley, C., Pilling, M. J., and Robertson, S. H.: MESMER: an  
880 open-source master equation solver for multi-energy well reactions, *J. Phys. Chem. A*, 116,  
881 9545-9560, <https://doi.org/10.1021/jp3051033>, 2012.

882 Gong, Y., and Chen, Z.: Quantification of the role of stabilized Criegee intermediates in the  
883 formation of aerosols in limonene ozonolysis, *Atmos. Chem. Phys.*, 21, 813-829,  
884 <https://doi.org/10.5194/acp-21-813-2021>, 2021.

885 Hofzumahaus, A., Rohrer, F., Lu, K., Bohn, B., Brauers, T., Chang, C. C., Fuchs, H., Holland, F.,  
886 Kita, K., Kondo, Y., Li, X., Lou, S., Shao, M., Zeng, L., Wahner, A., and Zhang, Y.:  
887 Amplified trace gas removal in the troposphere, *Science*, 324, 1702-1704,  
888 <https://doi.org/10.1126/science.1164566>, 2009.

889 Holbrook, K. A., Pilling, M. J., Robertson, S. H., and Robinson, P. J.: *Unimolecular reactions*, 2nd  
890 ed.; Wiley: New York, 1996.

891 Huang, H. L., Chao, W., and Lin, J. J. M.: Kinetics of a Criegee intermediate that would survive  
892 high humidity and may oxidize atmospheric SO<sub>2</sub>, *Proc. Natl. Acad. Sci. U.S.A.*, 112,  
893 10857-10862, <https://doi.org/10.1073/pnas.1513149112>, 2015.

894 Iyer, S., Reiman, H., Møller, K. H., Rissanen, M. P., Kjaergaard, H. G., and Kurtén, T.:  
895 Computational investigation of RO<sub>2</sub> + HO<sub>2</sub> and RO<sub>2</sub> + RO<sub>2</sub> reactions of monoterpene derived  
896 first-generation peroxy radicals leading to radical recycling, *J. Phys. Chem. A*, 122,  
897 9542-9552, <https://doi.org/10.1021/acs.jpca.8b09241>, 2018.

898 Iyer, S., Rissanen, M. P., Valiev, R., Barua, S., Krechmer, J. E., Thornton, J., Ehn, M., and Kurtén,  
899 T.: Molecular mechanism for rapid autoxidation in  $\alpha$ -pinene ozonolysis, *Nat. Commun.*,  
900 <https://doi.org/10.1038/s41467-021-21172-w>, 12, 878-883, 2021.

901 Jara-Toro, R. A., Hernández, F. J., Garavagno, M. A., Taccone, R. A., and Pino, G. A.: Water  
902 catalysis of the reaction between hydroxyl radicals and linear saturated alcohols (ethanol and  
903 n-propanol) at 294 K, *Phys. Chem. Chem. Phys.*, 20, 27885-27896,  
904 <https://doi.org/10.1039/C8CP05411H>, 2018.

905 Jara-Toro, R. A., Hernández, F. J., Taccone, R. A., Lane, S. I., and Pino, G. A.: Water catalysis of  
906 the reaction between methanol and OH at 294 K and the atmospheric implications, *Angew.  
907 Chem., Int. Ed.*, 56, 2166-2170, <https://doi.org/10.1002/anie.201612151>, 2017.

908 Jokinen, T., Sipilä M., Richters, S., Kerminen, V. M., Paasonen, P., Stratmann, F., Worsnop, D.,  
909 Kulmala, M., Ehn, M., Herrmann, H., and Berndt, T.: Rapid autoxidation forms highly  
910 oxidized RO<sub>2</sub> radicals in the atmosphere, *Angew. Chem. Int. Ed.*, 53, 14596-14600,  
911 <https://doi.org/10.1002/anie.201408566>, 2014.

912 Khan, M. A. H., Percival, C. J., Caravan, R. L., Taatjes, C. A., and Shallcross, D. E.: Criegee  
913 intermediates and their impacts on the troposphere, *Environ. Sci.: Processes Impacts*, 20,  
914 437-453, <https://doi.org/10.1039/C7EM00585G>, 2018.

915 Kumar, M., and Francisco, J. S.: Red-light initiated decomposition of  $\alpha$ -hydroxy methylperoxy  
916 radical in the presence of organic and inorganic acids: implications for the HO<sub>x</sub> formation in  
917 the lower stratosphere, *J. Phys. Chem. A*, 120, 2677-2683,  
918 <https://doi.org/10.1021/acs.jpca.6b01515>, 2016.

919 Kumar, M., and Francisco, J. S.: Red-light-induced decomposition of an organic peroxy radical: a  
920 new source of the HO<sub>2</sub> radical, *Angew. Chem. Int. Ed.*, 54, 15711-15714,

921 <https://doi.org/10.1002/anie.201509311>, 2015.

922 Kumar, M., Busch, D. H., Subramaniam, Bala., and Thompson, W. H.: Role of tunable acid  
923 catalysis in decomposition of  $\alpha$ -hydroxyalkyl hydroperoxides and mechanistic implications  
924 for tropospheric chemistry, *J. Phys. Chem. A*, 118, 9701-9711,  
925 <https://doi.org/10.1021/jp505100x>, 2014.

926 Lee, R., Gryn'ova, G., Ingold, K. U., and Coote, M. L.: Why are sec-alkylperoxyl bimolecular  
927 self-reactions orders of magnitude faster than the analogous reactions of tert-alkylperoxyls?  
928 The unanticipated role of CH hydrogen bond donation, *Phys. Chem. Chem. Phys.*, 18,  
929 23673-23679, <https://doi.org/10.1039/C6CP04670C>, 2016.

930 Lester, M. I., and Klippenstein, S. J.: Unimolecular decay of Criegee intermediates to OH radical  
931 products: prompt and thermal decay processes, *Acc. Chem. Res.*, 51, 978-985,  
932 <https://doi.org/10.1021/acs.accounts.8b00077>, 2018.

933 Liu, L., Bei, N., Wu, J., Liu, S., Zhou, J., Li, X., Yang, Q., Feng, T., Cao, J., Tie, X., and Li, G.:  
934 Effects of stabilized Criegee intermediates (sCIs) on sulfate formation: a sensitivity analysis  
935 during summertime in Beijing-Tianjin-Hebei (BTH), China. *Atmos. Chem. Phys.*, 19,  
936 13341-13354, <https://doi.org/10.5194/acp-19-13341-2019>, 2019.

937 Long, B., Bao, J. L., and Truhlar, D. G.: Reaction of SO<sub>2</sub> with OH in the atmosphere, *Phys. Chem.*  
938 *Chem. Phys.*, 19, 8091-8100, <https://doi.org/10.1039/C7CP00497D>, 2017.

939 Lu, T.: Molclus program, Version 1.9.3, <http://www.keinsci.com/research/molclus.html> (accessed  
940 Feb. 10, 2020).

941 Ma, F., Guo, X., Xia, D., Xie, H. B., Wang, Y., Elm, J., Chen, J., and Niu, J.: Atmospheric  
942 chemistry of allylic radicals from isoprene: a successive cyclization-driven autoxidation  
943 mechanism, *Environ. Sci. Technol.*, 55, 4399-4409, <https://doi.org/10.1021/acs.est.0c07925>,  
944 2021.

945 Møller, K. H., Berndt, T., and Kjaergaard, H. G.: Atmospheric autoxidation of amines, *Environ.*  
946 *Sci. Technol.*, 54, 11087-11099, <https://doi.org/10.1021/acs.est.0c03937>, 2020.

947 Møller, K. H., Otkjær, R. V., Hyttinen, N., Kurtán, T., and Kjaergaard, H. G.: Cost-effective  
948 implementation of multiconformer transition state theory for peroxy radical hydrogen shift  
949 reactions, *J. Phys. Chem. A*, 120, 10072-10087, <https://doi.org/10.1021/acs.jpca.6b09370>,  
950 2016.

951 Nozière, B., and Vereecken, L.: Direct observation of aliphatic peroxy radical autoxidation and  
952 water effects: an experimental and theoretical study, *Angew. Chem. Int. Ed.*, 58, 13976-13982,  
953 <https://doi.org/10.1002/anie.201907981>, 2019.

954 Orlando, J. J., and Tyndall, G. S.: Laboratory studies of organic peroxy radical chemistry: an  
955 overview with emphasis on recent issues of atmospheric significance, *Chem. Soc. Rev.*, 41,  
956 6294-6317, <https://doi.org/10.1039/c2cs35166h>, 2012.

957 Perring, A. E., Pusede, S. E., and Cohen, R. C.: An observational perspective on the atmospheric  
958 impacts of alkyl and multifunctional nitrates on ozone and secondary organic aerosol, *Chem.*  
959 *Rev.*, 113, 5848-5870, <https://doi.org/10.1021/cr300520x>, 2013.

960 Piletic, I. R., Edney, E. O., and Bartolotti, L. J.: Barrierless reactions with loose transition states  
961 govern the yields and lifetimes of organic nitrates derived from isoprene, *J. Phys. Chem. A*,  
962 121, 8306-8321, <https://doi.org/10.1021/acs.jpca.7b08229>, 2017.

963 Qiu, J. T., Ishizuka, S., Tonokura, K., Colussi, A. J., and Enami, S.: Water dramatically accelerates  
964 the decomposition of  $\alpha$ -hydroxyalkyl-hydroperoxides in aerosol particles, *J. Phys. Chem.*

965 Lett., 10, 5748-5755, <https://doi.org/10.1021/acs.jpcelett.9b01953>, 2019.

966 Rissanen, M. P., Kurtšn, T., Sipilä M., Thornton, J. A., Kangasluoma, J., Sarnela, N., Junninen, H.,  
967 Jørgensen, S., Schallhart, S., Kajos, M. K., Taipale, R., Springer, M., Mentel, T. F.,  
968 Ruuskanen, T., Petäjä T., Worsnop, D. R., Kjaergaard, H. G., and Ehn, M.: The formation of  
969 highly oxidized multifunctional products in the ozonolysis of cyclohexene, *J. Am. Chem.*  
970 *Soc.*, 136, 15596-15606, <https://doi.org/10.1021/ja507146s>, 2014.

971 Russell, G. A.: Deuterium-isotope effects in the autoxidation of aralkyl hydrocarbons. Mechanism  
972 of the interaction of peroxy radicals, *J. Am. Chem. Soc.*, 79, 3871-3877,  
973 <https://doi.org/10.1021/ja01571a068>, 1957.

974 Ryzhkov, A. B., and Ariya, P. A.: A theoretical study of the reactions of carbonyl oxide with water  
975 in atmosphere: the role of water dimer, *Chem. Phys. Lett.*, 367, 423-429,  
976 [https://doi.org/10.1016/S0009-2614\(02\)01685-8](https://doi.org/10.1016/S0009-2614(02)01685-8), 2003.

977 Smith, M. C., Chang, C. H., Chao, W., Lin, L. C., Takahashi, K., Boering, K. A., and Lin, J. J. M.:  
978 Strong negative temperature dependence of the simplest Criegee intermediate  $\text{CH}_2\text{OO}$   
979 reaction with water dimer, *J. Phys. Chem. Lett.*, 6, 2708-2713,  
980 <https://doi.org/10.1021/acs.jpcelett.5b01109>, 2015.

981 Stone, D., Whalley, L. K., and Heard, D. E.: Tropospheric OH and  $\text{HO}_2$  radicals: field  
982 measurements and model comparisons, *Chem. Soc. Rev.*, 41, 6348-6404,  
983 <https://doi.org/10.1039/c2cs35140d>, 2012.

984 Taatjes, C. A., Welz, O., Eskola, A. J., Savee, J. D., Scheer, A. M., Shallcross, D. E., Rotavera, B.,  
985 Lee, E. P. F., Dyke, J. M., Mok, D. K. W., Osborn, D. L., and Percival, C. J.: Direct  
986 measurements of conformer-dependent reactivity of the Criegee intermediate  $\text{CH}_3\text{CHOO}$ ,  
987 *Science*, 340, 177-180, <https://doi.org/10.1126/science.1234689>, 2013.

988 Taatjes, C. A.: Criegee intermediates: what direct production and detection can teach us about  
989 reactions of carbonyl oxides, *Annu. Rev. Phys. Chem.*, 68, 183-207,  
990 <https://doi.org/10.1146/annurev-physchem-052516-050739>, 2017.

991 Valiev, R. R., Hasan, G., Salo, V. T., Kubečka, J., and Kurten, T.: Intersystem crossings drive  
992 atmospheric gas-phase dimer formation, *J. Phys. Chem. A*, 123, 6596-6604,  
993 <https://doi.org/10.1021/acs.jpca.9b02559>, 2019.

994 Wang, S., Riva, M., Yan, C., Ehn, M., and Wang, L.: Primary formation of highly oxidized  
995 multifunctional products in the OH-initiated oxidation of isoprene: a combined theoretical  
996 and experimental study, *Environ. Sci. Technol.*, 52, 12255-12264,  
997 <https://doi.org/10.1021/acs.est.8b02783>, 2018.

998 Wang, S., Wu, R., Berndt, T., Ehn, M., and Wang, L.: Formation of highly oxidized radicals and  
999 multifunctional products from the atmospheric oxidation of alkylbenzenes, *Environ. Sci.*  
1000 *Technol.*, 51, 8442-8449, <https://doi.org/10.1021/acs.est.7b02374>, 2017.

1001 Wennberg, P. O., Bates, K. H., Crouse, J. D., Dodson, L. G., McVay, R. C., Mertens, L. A.,  
1002 Nguyen, T. B., Praske, E., Schwantes, R. H., Smarte, M. D., Clair, J. M. S., Teng, A. P.,  
1003 Zhang, X., and Seinfeld, J. H.: Gas-phase reactions of isoprene and its major oxidation  
1004 products, *Chem. Rev.*, 118, 3337-3390, <https://doi.org/10.1021/acs.chemrev.7b00439>, 2018.

1005 Winiberg, F. A. F., Dillon, T. J., Orr, S. C., Groß C. B. M., Bejan, I., Brumby, C. A., Evans, M. J.,  
1006 Smith, S. C., Heard, D. E., and Seakins, P. W.: Direct measurements of OH and other product  
1007 yields from the  $\text{HO}_2 + \text{CH}_3\text{C}(\text{O})\text{O}_2$  reaction, *Atmos. Chem. Phys.*, 16, 4023-4042,  
1008 <https://doi.org/10.5194/acp-16-4023-2016>, 2016.

1009 Xu, L., Kollman, M. S., Song, C., Shilling, J. E., and Ng, N. L.: Effects of NO<sub>x</sub> on the volatility of  
1010 secondary organic aerosol from isoprene photooxidation, *Environ. Sci. Technol.*, 48,  
1011 2253-2262, <https://doi.org/10.1021/es404842g>, 2014.

1012 Xu, L., Møller, K. H., Crounse, J. D., Kjaergaard, H. G., and Wennberg, P. O.: New insights into  
1013 the radical chemistry and product distribution in the OH-initiated oxidation of benzene,  
1014 *Environ. Sci. Technol.*, 54, 13467-13477, <https://doi.org/10.1021/acs.est.0c04780>, 2020.

1015 Zhang, D., Zhang, R., Park, J., and North, S. W.: Hydroxy peroxy nitrites and nitrates from OH  
1016 initiated reactions of isoprene, *J. Am. Chem. Soc.*, 124, 9600-9605,  
1017 <https://doi.org/10.1021/ja0255195>, 2002.

1018 Zhang, P., Wang, W., Zhang, T., Chen, L., Du, Y., Li, C., and Lv, J.: Theoretical study on the  
1019 mechanism and kinetics for the self-reaction of C<sub>2</sub>H<sub>5</sub>O<sub>2</sub> radicals, *J. Phys. Chem. A*, 116,  
1020 4610-4620, <https://doi.org/10.1021/jp301308u>, 2012.

1021 Zhao, Y., and Truhlar, D. G.: A new local density functional for main-group thermochemistry,  
1022 transition metal bonding, thermochemical kinetics, and noncovalent interactions, *J. Chem.*  
1023 *Phys.*, 125, 194101-194119, <https://doi.org/10.1063/1.2370993>, 2006.

1024 Zhao, Y., and Truhlar, D. G.: The M06 suite of density functionals for main group  
1025 thermochemistry, thermochemical kinetics, noncovalent interactions, excited states, and  
1026 transition elements: two new functionals and systematic testing of four M06-class functionals  
1027 and 12 other functionals, *Theor. Chem. Acc.*, 120, 215-241,  
1028 <https://doi.org/10.1007/s00214-007-0310-x>, 2008.

1029 Zheng, J., and Truhlar, D. G.: Direct dynamics study of hydrogen-transfer isomerization of  
1030 1-pentyl and 1-hexyl radicals, *J. Phys. Chem. A*, 113, 11919-11925,  
1031 <https://doi.org/10.1021/jp903345x>, 2009.

1032 Zheng, J., Xu, X., and Truhlar, D. G.: Minimally augmented Karlsruhe basis sets, *Theor. Chem.*  
1033 *Acc.*, 128, 295-305, <https://doi.org/10.1007/s00214-010-0846-z>, 2011.

1034 Zhong, J., Kumar, M., Francisco, J. S., and Zeng, X. C.: Insight into chemistry on cloud/aerosol  
1035 water surfaces, *Acc. Chem. Res.*, 51, 1229-1237,  
1036 <https://doi.org/10.1021/acs.accounts.8b00051>, 2018.

1037 Zhou, X., Liu, Y., Dong, W., and Yang, X.: Unimolecular reaction rate measurement of  
1038 *syn*-CH<sub>3</sub>CHOO, *J. Phys. Chem. Lett.*, 10, 4817-4821,  
1039 <https://doi.org/10.1021/acs.jpcllett.9b01740>, 2019.

1040 Zhu, C., Kumar, M., Zhong, J., Li, L., Francisco, J. S., and Zeng, X. C.: New mechanistic  
1041 pathways for Criegee-water chemistry at the air/water interface, *J. Am. Chem. Soc.*, 138,  
1042 11164-11169, <https://doi.org/10.1021/jacs.6b04338>, 2016.